5-2016

The Development of a Biomimetic Patch for Annulus Fibrosus Repair

Rachel Michelle McGuire
Clemson University, rmcguir@g.clemson.edu

THE DEVELOPMENT OF A BIOMIMETIC PATCH FOR ANNULUS FIBROSUS REPAIR

A Thesis
Presented to
the Graduate School of
Clemson University

In Partial Fulfillment
of the Requirements for the Degree
Master of Science
Bioengineering

---

by
Rachel Michelle McGuire
May 2015

Accepted by:
Dr. Jeremy Mercuri, Committee Chair
Dr. Dan Simionescu
Dr. Sonny Gill

ABSTRACT

Thirty-one million Americans experience low-back pain (LBP) at any given time in their lives.[1] LBP is the single leading cause of disability worldwide and its prevalence in the US is approximately 80%.[2] The intervertebral disc (IVD) is composed of the nucleus pulposus (NP), a gelatinous core that resists compressive loading through the generation of intradiscal pressure (IDP), and the annulus fibrosus (AF), which has concentric sheets (lamellae) of aligned Type I collagen which alternate the fiber-preferred direction with each subsequent layer allowing for resistance to IDP, and tensile and torsional loads. Although, IVD degeneration (IVDD) and herniation (IVDH) represent two independent pathological mechanisms; they both contribute significantly to LBP. Potential clinical treatments for herniation and degeneration include discectomy (removal of the herniated IVD fragments) and NP arthroplasty, respectively. However, both treatment options are insufficient by themselves; especially when the defect in the outer AF is >6mm.[3] We hypothesized that an ideal AF patch to be used for repairing the AF and promoting its regeneration can be developed from adjoined sheets of decellularized porcine pericardium due to its aligned type I collage fiber architecture resembling the native AF structure. The objective of the research presented herein was to illustrate the feasibility of developing a biomimetic patch to biologically augment AF repair.

Porcine pericardium was harvested at a local abattoir and decellularized in order to minimize potential immunological reactions.[4] Decellularization was confirmed via, Hematoxylin & Eosin (H&E), agarose gel electrophoresis, nanodrop quantification and immunohistochemistry for the removal of the porcine antigenic epitope, alpha-gal. Tensile

mechanical testing was performed on single-ply AF sheets and fresh pericardium in the fiber preferred and cross-fiber orientation to determine tensile mechanical properties and to compare values reported in literature for a single AF lamellae, and to ensure the modified decellularization procedure did not alter the mechanical strength of the tissue. Ball burst test of multi-laminate AF patches composed of decellularized pericardial layers was performed to assess the maximum burst strength the pericardium could withstand and the necessary number of layers needed to resist the IDP generated by the NP exerted as hoop stresses within the AF. Production of ply-angle-ply multi-laminate AF patches were constructed via the use of decellularized pericardium sheets were sewn in conjunction with a backing material, surgical suture and a sewing machine in order to develop a scalable manufacture methodology. Cytocompatibility of the AF patches was verified through a 15 day *in vitro* pilot cell study to assess bovine AF cell viability and proliferation when seeded on the patch.

Results to be presented illustrate a repeatable method for developing a multi-laminate ply-angle-ply AF patch. The AF patch demonstrates comparable tensile elastic modulus to native AF, adequate burst strength and cytocompatibility to be considered a potential option for AF tissue engineering. Taken together, results suggest that the multi-laminate ply-angle-ply AF patches may be suitable for use as an adjunct to nucleus arthroplasty implantation as an early-stage treatment for patients demonstrating the onset of IVDD or as a sequestration device in patients undergoing discectomy following large IVDHs to help mitigate the risk for re-herniation.

DEDICATION

This work is dedicated to my parents and my brother. I would like to express my sincerest gratitude for their love and continued support throughout the course of my life. Thanks Mom, Dad, and Thomas for all the encouragement and help along the way. You all have taught me so much, and I appreciate everything you have done for me.

ACKNOWLEDGMENTS

First, I would like to thank my advisor, Dr. Jeremy Mercuri, for his trust in my capabilities to conduct research within our laboratory (The Laboratory of Orthopaedic Tissue Regeneration and Orthobiologics). His kind words, guidance, support, and constant encouragement proved to be a great motivator and large influence in this work.

I would also like to thank all of my committee members; Dr. Sonny Gill and Dr. Dan Simionescu for their insight, constructive criticisms and advice in support of my project.

I am extremely appreciative to my two undergraduates for their vital help in completing my research on time. Specifically Ryan Borem, for his extensive after hours help and research. I would also like to thank all of my fellow researchers in the OrthO-X lab. Their collaborations, teachings and time spent helping me with my work made this project conceivable. Additionally their comradery also helped make this experience exciting and memorable. I want to wish you all the best of luck in your future endeavors.

I would also like to thank my fellow classmates and professors here in the Bioengineering department at Clemson. There is no other department I would rather be a part of due to the support and respect between the students and professors.

Thank you all of my family, friends and loves ones for their support throughout the years and for their constant guidance, unconditional love and support.

TABLE OF CONTENTS

Page

Table of Contents (Continued)

LIST OF FIGURES

List of Figures (Continued)

List of Figures (Continued)

CHAPTER 1

LITERATURE REVIEW

1.1 Clinical Significance: Intervertebral Disc Herniation & Degeneration

Thirty-one million Americans experience low-back pain (LBP) during their lifetime.[1] LBP is the single leading cause of disability worldwide, according to the Global Burden of Disease 2010, and its prevalence within the United States (U.S.) is approximately 80%.[2] It is estimated that Americans spend a minimum of $50 billion addressing LBP (i.e. pharmaceuticals, doctors' visits, and physical therapy) each year.[3] Back related conditions are an enormous economic burden, and are a frequent cause of disability leading to annual healthcare costs that exceed $1 billion in the U.S.[4] Back related conditions typically include pathologies of the intervertebral disc (IVD): herniation and degeneration. Greater than half of lumbar IVD herniation's occur in active individuals between age 20 - 40 years.[5] IVD herniation is most commonly treated by discectomy, and healthcare spending on lumbar discectomies for IVD herniation have been estimated to exceed $300 million annually.[6] Despite the 1,000,000 discectomy procedures performed annually, patient satisfaction is approximately 75% at 1 year. Roughly 19% of these patients need re-operation 9 years after the original procedure.[7,8] There is a critical overall risk of recurrent IVD herniation between 6%-24%,[9] particularly in patients with a AF defect that exceeds 6 mm[10]. Intervertebral disc degeneration (IVDD) is seen in approximately 20% of people in their teens and then increases steeply with age, particularly in males. Approximately 10% of 50-year-old IVD's and 60% of 70-year-old IVD's are

severely degenerate.[11] Spinal fusion based procedures have become the most common treatment for severe LBP caused by IVDD. About 87% of spinal procedures in 2013 were fusion-based, according to the research firm GlobalData and there were more than 465,000 fusion operations in the U.S. in 2011, according to the Agency for Healthcare Research and Quality (AHRQ).[12,13] The estimated cost of spinal fusion procedures were more than $12.8 billion in 2011, according to AHRQ.[13] However, spinal fusion may result in detrimental long term results, such as adjacent segment degeneration and reduced spinal range of motion.[14]

1.2 The Intervertebral Disc (IVD)

1.2.1 IVD Structure

The spine contains twenty three intervertebral discs (IVD's); six in the cervical region, twelve in the thoracic and five in the lumbar region. The largest IVD's are located in the lumbar region and are approximately 7-10 mm thick and 4 cm in diameter.[15] The IVD's are responsible for one fourth the total length of the spinal column. The IVD's are the primary structural unit located between the concave articular surfaces of the adjacent vertebrae.[16] Each individual IVD is made up of three distinct regions: the annulus fibrosus (AF), the nucleus pulposus (NP), and the cartilaginous endplate (CEP) (**Figure 1**). The AF is the outermost region of the IVD that consists of concentric sheets of collagen which provides structural support of the IVD and aids in its attachment to adjacent vertebral bodies. The NP is the gelatinous core of the IVD which generates an IDP inside the confined space of the AF. The CEP is a thin layer of articular cartilage that encompasses

the top and bottom of the IVD at the interface of the IVD and the adjacent vertebrae. The three major biochemical constitutents of the IVD are water, fibrillar collagens and aggrecan. The proportion and organization of these components vary considerably with

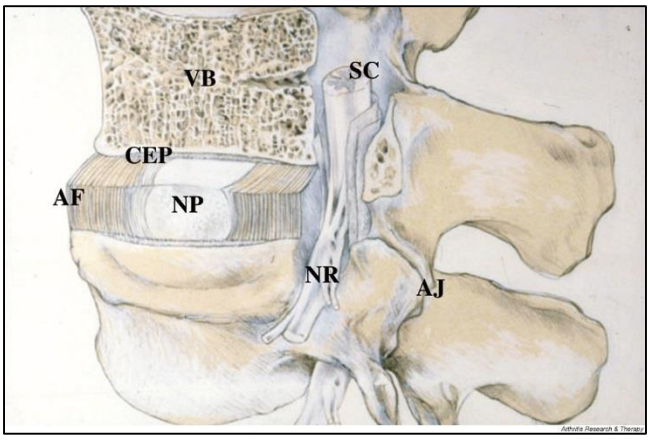

Figure 1: Structure of the intervertebral disc depicting the annulus fibrosus (AF), the nucleus pulposus (NP), and the cartilaginous endplate (CEP).[58]

position across the IVD with the NP having a higher concentration of water and the proteoglycan, aggrecan, than other regions of the IVD.[17] The IVDs are the largest avascular/aneral sturctures in the human body.[16] Since the IVD's are avascular they have a very low cell density in comparisson to other tissues, with cells occupying approximately 0.25-0.5% of the tissue volume. Although there are few cells, their role is vital as they are responsible for sythesizing and maintaining an appropriate macromolecular compostion. The activity of IVD cells can be regulated by growth factors, cytokines, and mechanical stress.

1.2.1.1 Nucleus Pulposus

The centrally located nucleus pulposus (NP) (**Figure 2**) contains randomly oriented network of collagen type II and elastin fibers (sometimes up to 150 μm in length), which are arranged radially; these fibers are embedded in a highly hydrated aggrecan-containing hydrogel.[15] The NP is gelatinous due to its high water and aggrecan content. The aggrecan is a large aggregating proteoglycan consisting of a protein core to which up to 100 highly sulphated glycosaminoglycan (GAG) chains, principally chondroitin and keratin sulphate, which are covalently attached.[17] The GAGs are highly negatively charged which attracts the binding of small positively charged cations into the tissue to balance the net charge. These ions then encourage the infiltration of water through osmosis into the NP. The water content can be as great as 85% in young people and decrease by 10 - 15% during aging.[18] This influx of water exerts an intradiscal swelling pressure on the collagen network (**Figure 2).** It's the retention of aggrecan and the low permeability of the NP extracellular matrix in compression within the collagen network that causes the swelling pressure reserved for resisting compressive load with minimal deformation.[19] In order to maintain osmotic equilibrium, fluid is expressed out of the NP as pressure increases, but because of the IVD's size and low hydraulic permeability, water loss is slow and returning to equilibrium takes many hours.[17] This unique resistances to compression from axial loading forces allows the NP to act as a shock absorber to prevent injury to the vertebral body.[16]

The cells within the NP are chondrocyte-like, being rounded and segregated from each other by the extracellular matrix (ECM).[17] The cells synthesize collagen type II and type X, express hypoxia-inducible factors, and secrete proteases and interleukins.[20]

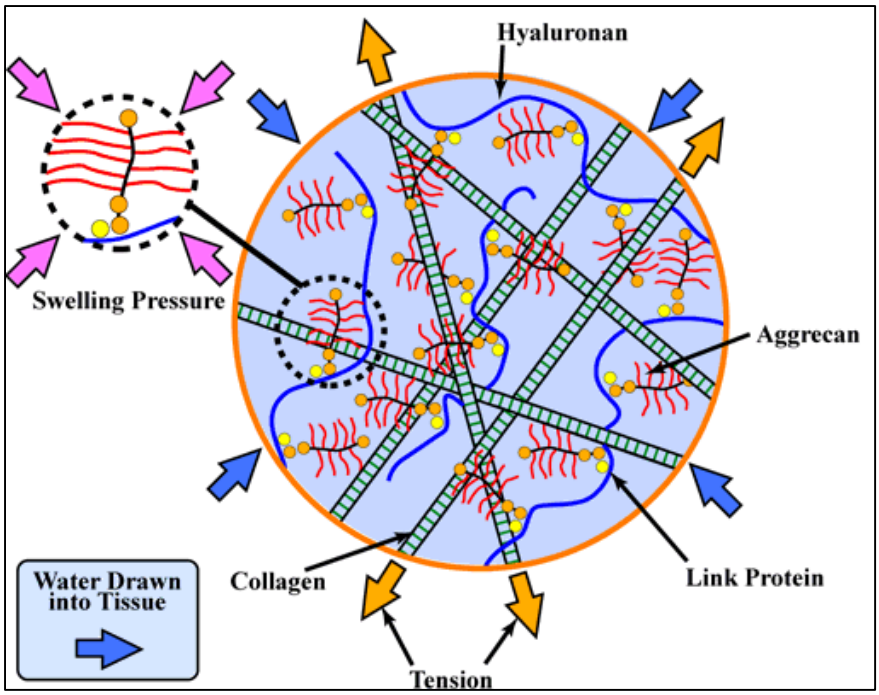

Figure 2: Depiction of the function of collagen fibers and proteoglycans in the nucleus pulposus.[59]

1.2.1.2 Annulus Fibrosus

The annulus fibrosus (AF) is made up of a series of 15–25 concentric sheets, or lamellae, with the collagen fibers lying parallel within each lamella. The fibers are orientated at approximately 30° to the horizontal axis, alternating direction with each adjacent lamellae (**Figure 3).**[15] The fiber alternating lamellae is commonly referred to as a ply-angle-ply architecture. The AF has a much higher collagen and lower water content as compared to the NP.[21] The AF consists of water (65-90%), collagen (50-70% dry weight), proteoglycans (10-20% dry weight) and non-collagenous proteins (e.g. elastin).[22]

The spaces between the lamellae are called interlamellar septae, and they contain proteoglycans, versican, and water that help decrease friction between the layers during movement of the spine. The lamellae are also interspersed with elastin fibers which help the IVD to return to its original arrangement following bending of the spine.[23] The outer AF lamellae are composed of majority type I collagen but type II collagen increases towards with inner lamellae. At the periphery, some of the annulus fibers pass the endplates to penetrate into the bone of the vertebral body in structures known as "Sharpey's fibers". This highly fibro-cartilaginous structure allows the AF to exhibit a complex anisotropic behavior to resist the forces exerted on it during compression, bending and tension.[22] The unique alignment of the fibers within each lamellae resists high tensile forces during

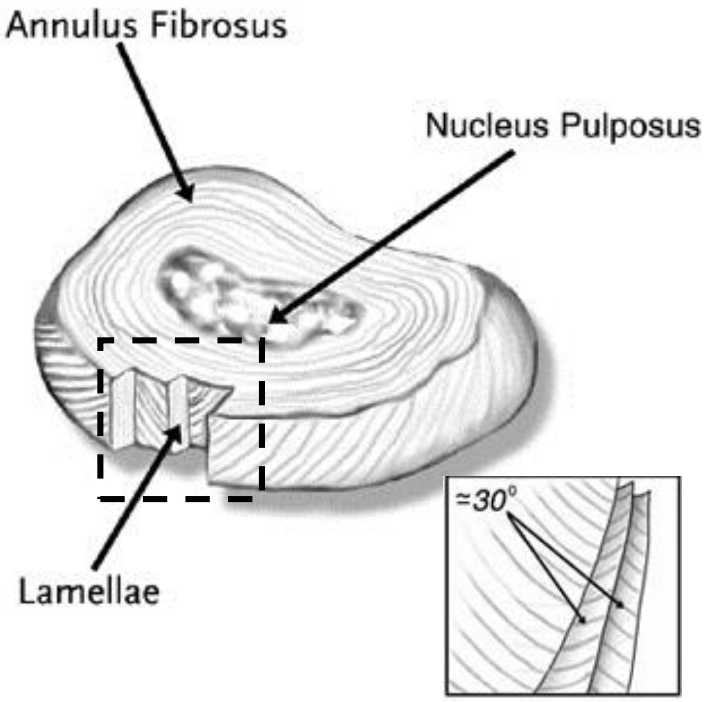

Figure 3: Depiction of the ply-angle-ply multi-laminate concentric sheets and the collagen fiber orientation within the annulus fibrosus.[60]

flexion or extension of the spine. The AF is responsible for the stable structure of the IVD during bending, twisting or compression of the spine.

The cells within the outer AF are thin and extend along the collagen fibrils, similar to tendon cells or fibroblasts. Towards the inner AF, the cells tend to have a more rounded morphology.[16] The AF cells have been shown to produce predominantly type I collagen and versican along with lesser amounts of type II collagen. Similar to the NP cells, they also respond to mechanical forces on the spine.

1.2.2 IVD Function

The human spine consists of 24 movable vertebrae that are stacked on top of one another, and joined through the IVD's. These interlocking vertebrae provide structure to the torso, and provide protection to the spinal cord nerve and nerve roots. Each IVD and its two adjacent vertebrae provide motion with six-degrees of freedom in flexion-extension,

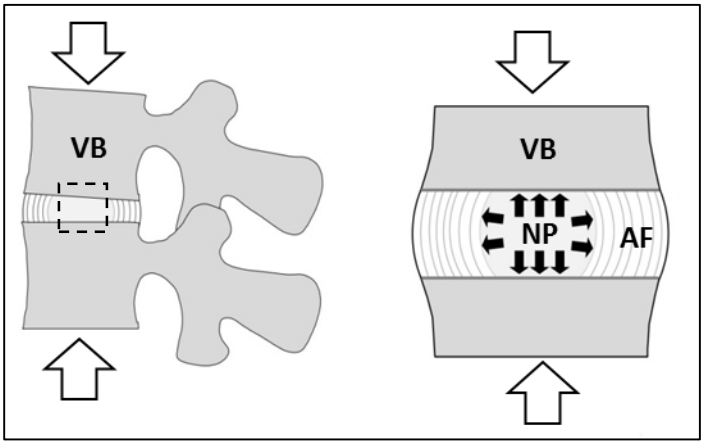

Figure 4: Schematic illustrating the compression of the nucleus pulposus (NP) and its redistribution of forces onto the annulus fibrosus (AF) and vertebral bodies (VB).

lateral bending, and axial rotation. The IVDs are flexible to allow for bending and twisting, but also act as shock absorbers during axial compression. This is done by keeping the vertebrae separated when under high compression forces. The structure of the IVDs is designed such that as the spine undergoes loading, it is resisted by the IDP generated by the confined NP. The NP then distributes pressure radially to the AF fibers generating hoop stresses within the AF and thus keeping the AF structure taut and therefore contributes to the stabilization of the function spinal units (***Figure 4***). The unique AF architecture is formed from 15-20 concentric layers of collagen sheets with an aligned ply-angle-ply orientation responsible for opposition of tensile and torsional loads generated during bending and twisting. When a compressive force is applied to the spine the IVD height gradually decreases as the load is dissipated, but over time it will regain its full height due to the hydrophilic properties of the NP. This is observed throughout the day as human height decreases due to constant muscle and gravitational forces creating compressive forces on the IVD's, but after sleeping throughout the night a person's height is restored. Typically, healthy IVD's are so strong that in compression, the vertebral body has the tendency to fail in compression before the IVD's rupture.[16]

1.3 IVD Herniation vs. Degeneration

1.3.1 Overview

Intervertebral disc herniation (IVDH) is a common condition that frequently affects the spine of young and middle-aged patients.[4] Majority of IVDH's are in young healthy IVD's between the ages of 20-40 years old. A herniated IVD, commonly known as a slipped or ruptured disc, occurs when the nucleus pulposus (NP) is extruded through some or all of the lamellae of the annulus fibrosus (AF) (**Figure 5**). It most frequently occurs in the lower back, specifically at the L1-L5 IVD's, and is the most common cause of low back pain (LBP), as well as leg pain (sciatica).[4] IVDH is commonly caused when a sudden and extreme load is exerted on a young, healthy spine. Herniation is directly related to the degree of degeneration of the IVD.[24] Due to the changes exhibited in the NP of a degenerated IVD (including NP dissection) only healthy or mildly degenerated IVD's can

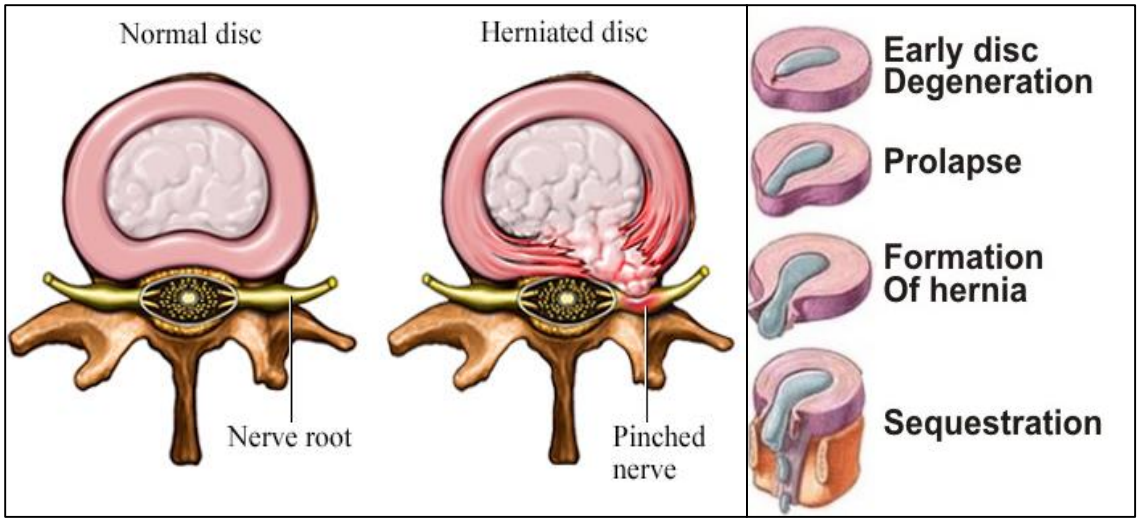

Figure 5: Depiction of a herniated disc (left) and stages of disc herniation (right).[61,62]

result in a herniation.[24] Causes of herniation may include accidents, such as car wrecks, work injuries, or sport related impacts. These injuries result in the IDP of the NP exceeding the strength of the AF lamellae resulting in the NP perforating between the fibers into the surrounding area of the spine. When the NP is extruded, the IVD height then decreases due to a loss of pressure inside the NP. The pressure is lost due to the decrease in NP material, and the ruptured AF can no longer support the IDP or compressive load. There are varying degrees of herniation (**Figure 5**), the first is prolapse, which is when the AF and NP extend into the surrounding area, but the NP has not broken through the last layers of the AF. The second type is a herniation where the NP has broken through all of the AF layers. The third type is sequestration where there are fragments of the NP that have broken off from the main herniation into the surrounding tissue. The extruded NP initiates the inflammatory cascade resulting in irritation to the surrounding nerves and tissues. All of these herniation types result in bulging into the surrounding tissue and have the potential to compress the nerve root**.** These herniation's can also cause a decrease in IVD height which may result in back pain and sciatica due to nerve root compression in between the vertebral foramina. Lumbar discectomy, removal of the extruding NP, is the most common surgical procedure performed for patients suffering from back pain and sciatica.[4] The procedure is performed despite exhibiting potential long term negative effects on adjacent vertebrae and IVD's. Discectomy is also associated with an increased risk of re-herniation when the AF defect is greater than 6 mm due to the inability of sutures to efficiently close the defect.[25] This surgical procedures effectiveness could be improved with the use of an AF closure device.[4]

As the body ages, the IVD ages naturally which slowly alters the natural biochemical composition of the IVD, and its biomechanical ability to resist compressive forces. By allowing the IVD to experience excessive mechanical loading, this can rapidly alter the biochemical composition of the spine leading to IVD degeneration (IVDD) (**Figure 6**). IVDD commonly initiates in the NP resulting in an altered stress distribution during compression from the NP to the AF which ultimately damages the entire functional spinal unit. IVD degeneration is a cell mediated process dependent on mechanical loading of the spine, age, genetics, biochemical influences, and smoking.[26] Evidence of spinal degeneration is present in between 90%-100% of individuals over the age of 63.[26] Degeneration implies a degradation of structure and/or function that is superimposed on top of the normal ageing process.[27] Stimuli such as increased load, osmotic pressure, and reduced glucose have shown to lead to altered cell function, resulting in cells that not only stop dividing and replicating, but increase production of cytokines and matrix-degrading enzymes. These enzymes of the metalloproteinase (MMP) family, are all capable of

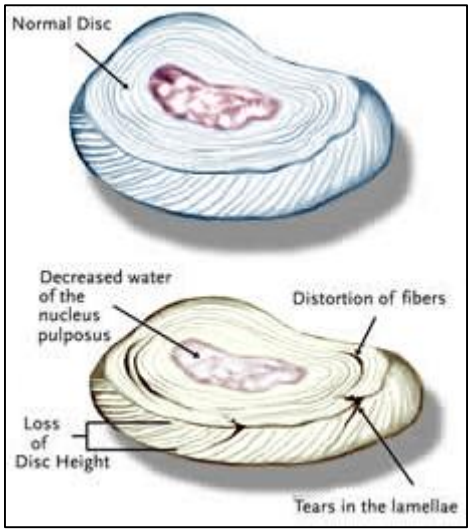

Figure 6: Depiction of disc degeneration.[63]

degrading proteoglycans and collagen, resulting in the loss of GAGs and IVD function. Cellular production of MMPs is supported by an acidic environment (such has been reported in degenerate IVD's), while GAG synthesis is drastically reduced, thereby leading to a vicious spiral of degeneration because matrix construction is outpaced by its destruction.[26] IVDD leads to a decreased IVD height which can result in nerve root impingement causing pain in patients' back and/or limb. The most common surgical solution for IVDD is spinal fusion. Spinal fusion is an end-stage treatment used in patients with debilitating pain and spinal instability. In recent years, there has been 6-fold increase in the number of spinal fusions performed, which is alarmingly high.

1.3.2 Surgical Solutions & Shortcomings

LBP and sciatica symptoms are initially treated with over-the-counter pain relievers and muscle relaxants.[28] Depending on the severity, antidepressants and prescription pain medication can be used for more severe and chronic pain.[28] If pain persists for at least six weeks despite treatment, patients are commonly referred to a specialist. From there a specialist generally prescribes an MRI to more accurately evaluate the potential causes of the patients' symptoms. Dependent on what is depicted in the MRI the specialist discusses potential physical therapy and surgical options. MRI images can show IVDD due to the decrease in water content resulting in the IVD to be blacker (***Figure 7***). MRI images can also show IVDH due to the NP perforating out past the AF edges and into the surrounding tissue (***Figure 7***).[23] IVDD and IVDH have some separate and overlapping treatment options. The most common treatment option for IVDH is lumbar discectomy, the removal

of the herniated NP.[29] Despite high rates of safety and success in relieving pain and improving function, between 10% and 30% of discectomy patients continue to experience unsatisfactory results such as a loss of IVD height and recurrent IVDH.[29] In order to mitigate re-herniation rates, traditionally a discectomy with removal of as much NP as possible was recommended. This has been shown to lead to long term IVD disruption due to loss of IVD height which transfers loads radially to the AF and facet joints.[18,30] In response to these long term effects, a limited discectomy was proposed to only remove the extruding NP without the internal NP. This led to an increased incidence of re-herniation. It has been shown that the rate of re-herniation after limited discectomy was greatest in patients with a large AF defect, > 6mm.[25] Currently, it has been suggested that a barrier or patch to close these large AF defects should be implemented to potentially reduce the high re-herniation rates.

Another potential surgical treatment for IVDH is the implementation of a NP replacement. An NP replacement could increase IVD height and restore compressive resistance to the IVD. A common concern with NP replacements is the process of inserting them into the IVD creates a defect in the AF. Due to this defect the use of NP replacements have been limited because of the potential to migrate out of the IVD. In order to utilize NP replacements a restraining structure is required inside the IVD. If the AF defect could be contained with a barrier or patch, an NP replacement could be implemented more readily. NP replacements are also being investigated for the treatment of IVDD. Since IVDD leads to a loss of functional NP and IVD height, an NP replacement could help mitigate those problems as an early stage intervention. IVDD is most commonly treated with spinal fusion

which is a destructive end stage treatment. Spinal fusion requires the complete removal of the degenerated IVD and the insertion of a spacer (synthetic or autologous bone) to keep adjacent vertebrae appropriately spaced in the absence of the IVD. Spinal fusion has been shown to lead to long term negative effects on adjacent IVD's due to unnatural loading which results in increased IVDD at adjacent levels.

***Figure 7**: MRI of normal, degenerated, and herniated IVD's.*[64]

Also on the market are medical devices specific for the closure of annular defects for after IVDH and discectomy. Devices similar to Xclose ™ from Anulex Technologies Inc. (Minnetonka, MN, USA) use a system of sutures to attempt to close the annular defect and restore IDP. The Xclose consists of two non-absorbable braided surgical 3-0 sutures and T-anchor assemblies, connected together with a loop of 2-0 suture. The 2-0 suture loop

is used to facilitate tightening, drawing the 3-0 suture assemblies together, thereby re-approximating the tissue.[31] While sutures do provide closure of the defect edges they do not create a sealed edge to completely prevent IDP leakage and therefore cannot reestablish the necessary IDP.[32] They are also limited in stability by the integrity of the adjacent annular structure. Other devices take a different approach, like the Barricaid annular closure device by Intrinsic Therapeutics Inc. (Woburn, MA) which acts as a 'plug' in the annular defect to reestablish the integrity of the AF. It is composed of a multi-layer, flexible, woven polyester mesh with a titanium anchor which is fixed to the proximal endplate.[33] The Barricaid has been shown to almost restore IVD height but does not allow for tissue regeneration or remodeling.

Current research suggests that treatment options for both IVDD and IVDH could be improved through the use of a patch for an intact AF in adjust with a NP replacement to restore IVD function. This treatment combination could be used for IVDH after discectomy to restore IVD height and prevent re-herniation. It could also be used in IVDD to restore IVD height and decrease associated pain with nerve root impingement.

1.4 AF Tissue Engineering

1.4.1 Overview

Tissue engineering (TE) of the IVD is an up and coming field, but it is still in its early stages. Many areas are being rapidly researched to find the best solution for repairing/regenerating/replacing all or part of the IVD. Current areas of interest are cell-

based therapies, graft transplants, and engineered scaffolds. IVD graft transplants seem most promising but allografts are not an option due to a limited donor supply of healthy discs because most IVDs have some form of degeneration by the age of 60, and also have the potential to transmit disease.[34] When engineering an IVD scaffold it is vital to remember the NP and AF perform very different functions and will most likely require two separate materials to satisfy these functions. Previous research has shown promising results for NP replacements however, TE of the AF has proved to be challenging due to its highly aligned architecture. An AF scaffold needs to mimic the biological characteristics of the native AF with a highly aligned ply-angle-ply multi-laminate architecture. This architecture is crucial for the scaffold to have suitable mechanical strength when comparing it to the native AF. The scaffold should withstand spinal bending, torsional forces and IDP generated inside the NP. The scaffold should allow for normal spinal motion and not disrupt adjacent vertebra or IVD's. This must all be maintained while also being cytocompatible. The scaffold needs to allow for cell viability, proliferation, and promote tissue regeneration/remodeling by those cells. A major concern is the lack of nutrients in the IVD environment, and its potential effect on these cells inside the scaffold which still needs to be addressed. Currently, most research is focused on a combination of the scaffolds and cells.

1.4.2 Cell Sources

The ideal cell source would be healthy autologous cells, but this is not always the most feasible option depending on the application. Human AF cells are difficult to come

by because IVD's are not readily available. Autologous AF cells are only harvested when there is an injury to the IVD and surgery is necessary, but due to the injury these cells are commonly unhealthy and do not make a reliable cell source.[35] Human AF cells can also be harvested from allogeneic sources, such as donated human IVD's, although it is rare these IVD's do no exhibit some degree of IVDD. Allogeneic AF sources raise new concerns such as the spreading of diseases and potential immunological reactions. Another potential AF source is xenogeneic cells, most commonly from bovine, porcine, rabbit, and sheep IVD's. These cells are most commonly used for in vitro studies in place of human AF cells since they are much more readily available. The animal AF cells allow researchers to determine how their device would react with native or stem cell derived AF cells. These cell are still not a viable option for implantation due to their immunological reactivity in humans. Another consideration when using AF cells is the difficulty when culturing inner and outer AF cells. It has been shown after 2 weeks in 2D culture AF cells lose their distinguishable phenotypes.[35] Although 3D culture helps cells stay differentiated, AF cells do not survive well in synthetic materials such as alginate.[35] In order for AF cells to be a viable option in AF tissue engineering there are still many barriers that need to be overcome.

A common cell source used in tissue engineering is stem cells. Stem cells are often a viable choice due to their differentiation capabilities and the reliable ability to harvest them. Until recently, stem cell focus has been on adult mesenchymal stem cells harvested from bone marrow until new breakthroughs in adipose derived stem cells have been made. Stem cells have the potential to differentiate into specific cells if they are presented with

the appropriate chemical and mechanical signals. Research is still being performed on the exact type of signals that will result in an AF cell phenotype in addition to determining discriminatory AF phenotypic markers. If the stem cells are implanted into native or decellularized tissue, it is presumed that the environmental signals will guide the cells to the AF cell phenotype and it is thought that four genes: collagen type I & II, aggrecan, and sox-9 could be used as an indicator of end stage AF cell phenotype.[36]

1.4.3 Scaffolds

Scaffolds can be considered any 3D structure that provides the structural support for cell attachment and subsequent tissue development.[37] Successful scaffolds allow for cell attachment and migration, deliver and retain cells and biochemical factors, enable diffusion of vital cell nutrients and expressed products, and exert mechanical and biological influences to modify the behavior of the cell phase. Scaffolds investigated for AF tissue engineering are composed of either synthetic or natural materials. Both natural and synthetic scaffolds must take into account immunogenicity, architectural and mechanical properties, biocompatibility and biodegradability, and method of graft delivery.[38] Macroscopically an AF scaffold provides a structural matrix to support and distribute mechanical loads and should mimic the unique ply-angle-ply architecture of the multi-layered AF. Microscopically an AF scaffold provides a provisional matrix in a three-dimensional microenvironment, to localize cells for cellular and molecular interactions appropriate for cell survival and differentiation. These are two distinct features that must both be considered when attempting to create an ideal AF scaffold.

An emerging area for AF scaffold formations is through the method of electrospinning. Electrospinning is a process in which a charged polymer jet is collected on a grounded collector; a rapidly rotating collector results in aligned nanofibers.[39] Electrospinning is advantageous for nanofibrous scaffolds due to the ability to highly align the nanofibers. Electrospun scaffolds are one of the few possibilities to actually exhibit a similar repeatability of the native AF architecture. Mimicking the native architecture is key since function follows structure it exhibits mechanical properties approximate that of a single AF lamella. A proposed benefit of the nanofibrous scaffold is its biodegradation, but matching the rate of ECM production by cells with the scaffolds degradation rate is a delicate balance. One that needs to be vetted by further research. Additional shortcomings of using the electrospinning technique arise when trying to develop an entire AF construct. The spun scaffold is developed in sheets ~1 mm in thickness which must be fixed together to mimic the unique ply-angle-ply multi-laminate AF structure. Current literature does not address this possible fixation method, or its potential to withstand significant compression under spinal loading. Overall, electrospinning is a tedious and challenging method to prefect, and it is not yet scalable to manufacturing size for marketing potential. Its potential is present, although, more research must be done in order to present it as a viable AF scaffold option.

Other proposed scaffolds exhibit similar pitfalls which need to be addressed. For example, porous silk fibroin scaffolds from silk worm cocoons have been shown to completely degrade *in vivo* in 2 years.[40] The degradation time would need to be investigated based on the native environment in the spine to ensure appropriate cellular ECM deposition

during that time. Silk fibroin also does not mimic the native ply-angle-ply AF structure and would need evaluation of its mechanical effects on the spines' dynamic loading. . A poly glycolic/lactic acid (PGA/PLA) copolymer scaffold have also been investigated, however, these constructs do not exhibit similar architecture to the native AF and has been shown to lose its rigid formation after only 12 weeks in an in vivo environment.[41] Again, a poly-D-L-lactide (PDLLA)/Bioglass, biodegradable poly(1,8-octanediomalate), and chitosan AF scaffolds do not exhibit a similar architecture to the native AF.[42–44] For an AF scaffold to be implemented it should: 1) fill and/or repair the AF defect in order to contain the NP, 2) allow fixation to the remaining AF, 3) allow for AF cell (or stem cell) viability, proliferation and ultimately differentiation in order to synthesize and secrete the appropriate ECM, 4) possess the characteristics anisotropic behavior of the native AF, 5) maintain/restore the mechanical properties of the spinal motion segment, while 6) not irritating or causing adhesions to adjacent spinal structures including the perineurium.[45] Current proposed solutions only focus on overall mechanical properties but not the influence of the properties on the surrounding native tissue, i.e. the innate need for a ply-angle-ply multi-laminate architecture to appropriately redistribute mechanical forces throughout the spinal unit. Proposed materials also do not report fixation methods to surrounding tissues, and are commonly only in the beginning stages of investigation. In summary, AF tissue engineering while it has promise, also holds many challenges to researchers. The current challenges is in developing a scalable method to manufacture a multi-laminate device that mimics the native architecture and strength of the AF. The native AF architectures is responsible for distributing forces through the spinal unit without

negatively impacting surrounding tissue and is needed in an AF tissue engineered replacement.

1.5 Towards the Development of a Biomimetic AF Patch

1.5.1 Justification

Current surgical treatments of patients with large AF herniation defects do not offer long term beneficial solution. After discectomy, patients are commonly left with an increased risk of re-herniation or negative side-effects to adjacent IVD's. In order to reduce these negative effects which can arise from discectomy, the patient's need an intact AF. Therefore, these patients would benefit from having an AF patch to reinforce the defect zone to help mitigate the risk of re-herniation after discectomy.

Current treatments for IVDD are invasive end-stage treatments with potentially detrimental long term results, including, adjacent segment degeneration in the case of spinal fusion, and altered biomechanics and implant subsidence and migration in the case of total IVD arthroplasty. Potential early-stage intervention treatments for IVDD are being developed (i.e. NP arthroplasty); however, in order to effectively implement such a technique, the AF needs to be intact. Taken together, patients' suffering from IVDH and IVDD may gain significant benefit from having a biomimetic AF patch available.

1.5.2 Project Goal & Aims

The goal of this project is to develop a biomimetic patch that will biologically augment AF repair. To achieve this goal, three specific aims were undertaken.

Aim #1: To develop and characterize a biomimetic AF scaffold via the decellularization of porcine pericardium.

Hypothesis: It was hypothesized that decellularized porcine pericardium would make an ideal AF patch given its natural, fiber aligned collagen sheet architecture, and to assess the tensile mechanical properties of single-ply decellularized pericardial sheets.

Approach: A) Porcine pericardium was harvested and decellularized via chemical methods. Removal of porcine cellular remnants, DNA, and the antigenic epitope alpha-gal was assessed via histology, DNA quantification, agarose gel electrophoresis, and immunohistochemistry, respectively.

B) Multi-axial burst strength testing and uniaxial tensile testing in the fiber preferred and cross-fiber direction was performed on single sheets of decellularized porcine pericardium.

Aim #2: To fabricate a multi-laminate scaffold with a fiber oriented direction.

Hypothesis: It was hypothesized that porcine pericardium sheets could be arranged in a ply-angle-ply architecture, and assembled into a multi-laminate patch which mimics the native structure of the human AF.

Approach: A) An AF patch formation method was developed.

B) Fiber orientation of the ply-angle-ply multi-laminate construct was evaluated.

C) Burst and suture retention strength of multi-ply AF patches were evaluated.

Aim #3: To assess the cytocompatibility of the AF patch with representative AF cells.

Hypothesis: It was hypothesized that the AF patch will support AF cell viability and proliferation.

Approach: A) Primary AF cells were isolated from bovine AF tissue and expanded for experimentation.

B) An *in vitro* pilot study was performed to assess AF cell viability, proliferation, and infiltration on multi-ply AF patches.

CHAPTER TWO

MATERIALS AND METHODS

2.1 Materials

Agarose (Low-EEO/Multi-Purpose/Molecular Biology Grade), Ethidium Bromide (1% Solution/Molecular Biology), exACTGene DNA Ladder, Deoxycholic Acid Sodium Salt (≥ 99%), 1 mM Ethylenediaminetetraacetic Acid (EDTA), Sodium Azide, Phosphate Buffered Saline (PBS) Tablets, Antibiotic/Antimycotic (Ab/Am), Dulbecco's Modification of Eagle's Medium (DMEM) were all purchased from Fisher Scientific (Fairlawn, NJ). Ethyl Alcohol (ETOH), Peracetic Acid Solution (32 wt. % in dilute acetic acid), and Hydroxyproline Assay Kit were all purchased from Sigma-Aldrich Corporation (St. Louis, MO). Proteinase K-solution (≥ 610 units/ml), Collagenase Type I (300 u/mg), Ribonuclease A (≥ 97.1 Ku units/mg), and Deoxyribonuclease I (≥ 3,480 u/mg DW) were all purchased from Worthington Biochemical Corporation (Lakewood, NJ). LDH Cytotoxicity Assay Kit was purchased from Pierce Biotech (Rockford, IL). DNeasy Blood & Tissue Kit was purchase from Qiagen. Tris (Hydrxmthl) Aminometh 50mM, Triton 100-x, and Dimethyl Sulfoxide (DMSO) were all purchased from VWR Scientific (Radnor, PA). Trizol and Picogreen dsDNA Assay Kit were all purchased from Life Technologies (Carlsbad, CA). Fetal Bovine Serum (FBS) (premium heat inactivated) was purchased from Atlanta Biologicals (Norcross, GA).

2.2 Methods

2.2.1 Porcine Pericardium Harvest & Decellularization

Decellularization procedure was adapted and modified from methods described by Tedder et al.[46] Porcine pericardium was collected at the time of slaughter from a local abattoir. Excess connective tissue and extraneous adipose tissue were removed from the pericardium using manual separation with tweezers and scalpel blades. All pericardium were then placed in 1-2 beakers of distilled water (ddH_2O) overnight and refrigerated at 4^oC for cell lysis. Decellularization of pericardium was done to remove cellular DNA in order to mitigate the native immune response within a patient's native environment.

Decellularization solution contained 50mM Tris, 0.15% Triton x-100 (v/v), 0.25% Deoxycholic acid-sodium salt, 0.1% 1 mM Ethylenediaminetetraacetic acid (EDTA), 0.02% Sodium Azide (NaN_3) (pH 7.8). After cells were lysed overnight using hypotonic solution, all tissues were rinsed once in fresh ddH_2O, and drained using a metal strainer. The tissues were then separated out into multiple specimen cups (~3 pieces of tissue per cup dependent on size of tissue pieces), and 100 ml of decellularization solution was added to each specimen cup. The cups were labeled and placed on a shaker at 150 rpm at room temperature for 3 days. After 3 days, the tissues were drained, and 100 ml of fresh decellularization solution was added to each specimen cup. The cups were returned to the shaker at room temperature for another 3 days. Following the 6 day period, the decell solution was discarded, and the tissues were rinsed in a series of washes for a total of 1 hour. Each specimen container was first washed for 10 minutes in 100 ml of ddH_2O at

room temperature on the shaker, and repeated once. The second wash was for 10 minutes in 100 ml of 70% Ethanol (ETOH) at room temperature on the shaker, and repeated once. The third wash was for 10 minutes in 100 ml of ddH_2O at room temperature on the shaker, and repeated once. Between each wash the tissue was drained using a metal strainer, and the used solution was discarded. Next, an increased concentration of DNase/RNase solution was prepared with DNase (stock = 3480 u/mg) 720 munits/ml, RNase (stock = 97.1 u/mg) 720 munits/ml dissolved in the appropriate amount of PBS with 5 mmol concentration of Magnesium chloride (MgCl) (pH of 7.5). Then 100 ml of DNase/RNase solution was added to each specimen cup. The cups were then placed in a 37^oC incubator/water bath with a shaker at 150 rpm for 24 hours. After 24 hours, the tissues were rinsed by inverting tubes back and forth 12 times, and were strained twice in 100 ml of ddH_2O. The tissue was then sterilized in100 ml of 0.1% Peracetic Acid in PBS (pH 7.4) for 2 hours on a shaker at 150 rpms at room temperature. All tissues were then rinsed in 100 ml of sterile PBS with changes every 30 minutes for a total of 2 hours on shaker at 150 rpms. The tissues were then combined into one pee cup and stored in 100 ml of 0.02% sodium azide in PBS (pH 7.4) at 4^oC until use.

2.2.2 Quantification of Pericardial Decellularization

Efficacy of decellularization was assessed by quantifying the amount of residual porcine DNA using agarose gel electrophoresis and nanodrop spectrophotometry. A Qiagen DNeasy Blood and Tissue Kit was used to extract total genomic DNA from both decellularized and fresh pericardium samples according to manufactures instructions.

(n=6/per group). Performing the agarose gel electrophoresis required two buffers: 10x TBE Buffer (Tris, Boric Acid and 1mM EDTA) and an Electrode Buffer (10x TBE and dH_20). Formation of the 1% agarose gel (10x TBE, dH_2O and Agarose) was done by microwaving the agarose gel until clear (~2 min) and then allowed to cool to 60^oC. Ethidium Bromide was then added to the mixture before being poured into the gel mold. The comb was inserted and air bubbles were pushed to the edge of the gel. Samples were prepared by adding 5 µL of 6X loading dye to each 30 µL sample of DNA in a 2 ml microfuge tube. Samples were centrifuged before loading in the agarose gel. The hardened gel was placed into electrophoresis container with wells closer to the negative terminal. The chambers of the container were filled with Electrode Buffer until the gel was completely submerged. 30 µL of the Standard DNA Ladder was loaded into the first lane of the gel with 30 µL of DNA sample in each of the following lanes. The gel was run at 100 V, 58 mA for 60 min and then the results were read.

2.2.3 Tensile Mechanical Testing of Pericardial Sheets

Mechanical tensile testing was performed on fresh and decellularized pericardium separated into two specific study groups. The representative samples in the first group were cut from pericardial sheets in the fiber preferred direction (parallel with the fibers) while the second group was cut in the cross-fiber direction (perpendicular to the fiber direction) (**Figure 8**). A sample size of n=6 for each type of pericardium in each group was tested. The tensile testing protocol was adapted from protocols used to test single human AF lamellae for tensile elastic modulus[47–49]. Tensile testing was done to ensure comparable

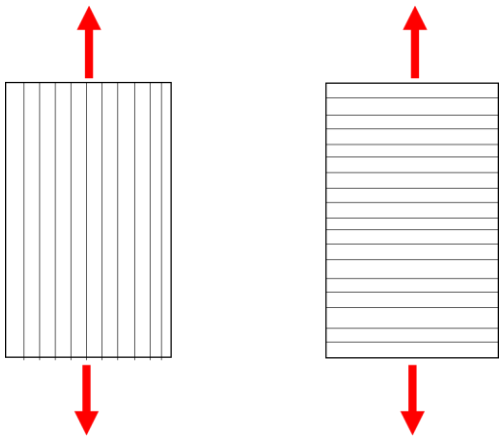

Figure 8: Images depicting the two groups of pericardium samples. (Left) Fiber preferred direction. (Right) Cross-fiber direction.

tensile elastic modulus to native human AF tissue. This is crucial to ensure the patch does not disrupt the function of the native tissue.

All testing was done on a mechanical testing system (MTS) with a 100 N load cell. The samples were first preheated to 37^{o}C in a water bath for 30 minutes before testing. The samples' length, width, and thickness were all determined before testing using digital calipers and ImageJ software (**Figure 9A**). The samples were prepped for testing by attaching sandpaper to the ends of each sample before insertion into the MTS clamps to prevent slipping (**Figure 9B)**. Once inserted into the testing setup the samples were preconditioned to 1 N with cyclic loading and tested to failure at a rate of 1 mm/min. Stress strain data was recorded and plotted. The tensile elastic modulus was determined from the linear region of the graph between 0.05 and 1.0 strain.

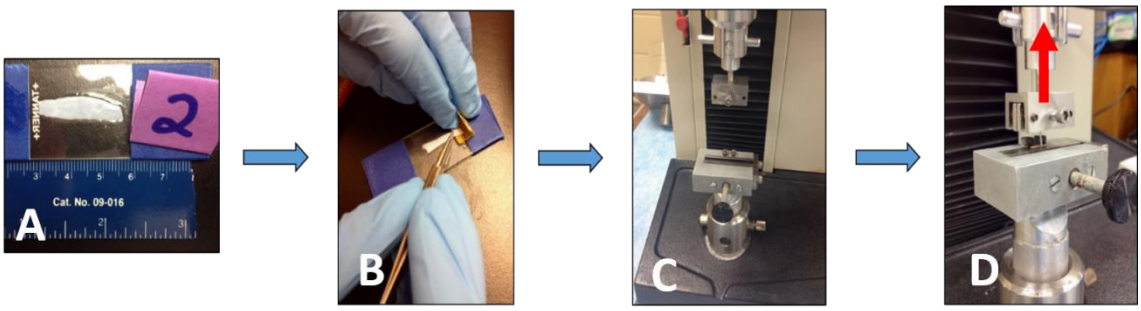

Figure 9: Representative images of MTS tensile testing setup process. (A) Determining the length and width of the specimens. (B) Prepping samples with sand paper on both ends to prevent slipping during testing. (C) Image of MTS machine fixture setup. (D) Image of tissue sample within testing setup.

2.2.4 Ball Burst Mechanical Testing of Single and Multi-layer Pericardium

The ball burst mechanical test was performed to determine the appropriate burst strength, and the number of layers needed to withstand the IDP. The burst strength of

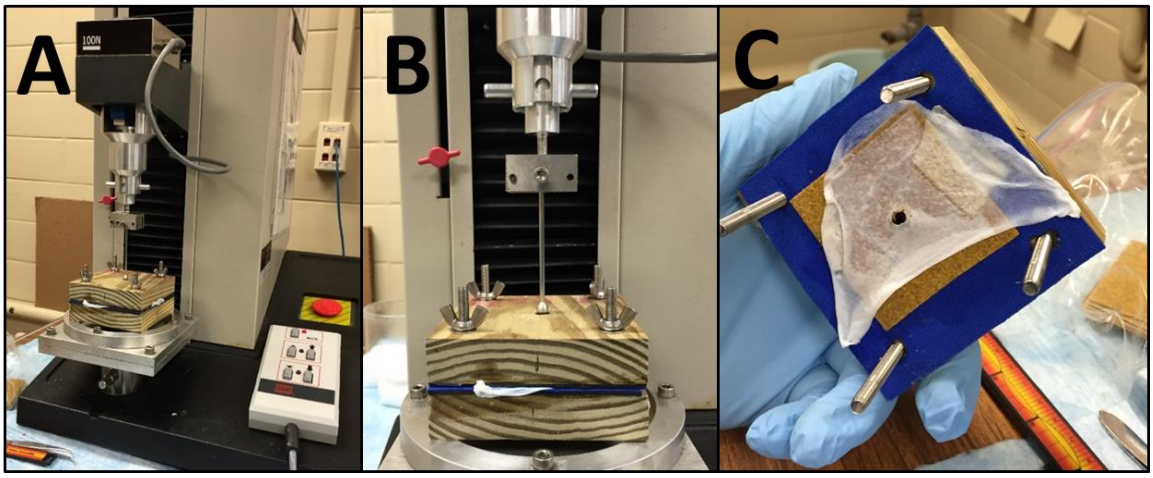

Figure 10: (A) The MTS ball burst setup. (B) Close-up of ball and rod before entering clamped tissue system. (C) Tissue after it had been burst by the ball.

decellularized pericardium sheets was determined using an Instron with a 1000N load cell. The ball burst strength testing protocol was adapted from the ASTM D3786/D3786M: Bursting Strength of Textile Fabrics Method. A custom designed testing fixture was made to hold the pericardium sheets during testing (**Figure 10**). The testing apparatus was two wooden blocks bolted together with a 6.25 mm diameter hole drilled through the center of both blocks. On the inside surface of each block a neoprene square was glued down with epoxy along with a layer of sandpaper to prevent the samples from slipping during testing. The pericardium samples were centered over the hole in the block and bolted together. A 6 mm steel ball and rod was attached to the Instron head and was used to burst the pericardium until failure under compression through the hole in the center of the testing apparatus (**Figure 10**). Pericardium samples of 1, 2, 3 and 6 layers were tested with n=6 in each group. The protocol recorded the displacement and the load the Instron head exerted on the pericardium until failure. The load the Instron exerted onto the pericardium was used to calculate the pressure the pericardium layers could withstand. In **Figure 11**, a is

the calculated contact surface [m] of the ball with the pericardium. F is the load [N] that the Instron exerted on the pericardium at the time of burst. R_1 and R_2 were the radius [m] of the ball (3 mm) and the pericardium (∞) respectively, where the pericardium was considered a sphere with an infinitely large radius. E_1 and E_2 were the elastic modulus [Pa] of the ball (200 GPa) and the pericardium (27 MPa, determined from tensile testing), respectively. ν_1 and ν_2 were the poisson's ratio of the ball (.27) and the pericardium (.3), respectively.[50–52] p_{max} was the maximum pressure [Pa] at the moment of burst of burst of the pericardium.

$$a = \sqrt[3]{\frac{3\,F\left[\frac{1-\nu_1^2}{E_1}+\frac{1-\nu_2^2}{E_2}\right]}{4\left(\frac{1}{R_1}+\frac{1}{R_2}\right)}}$$

$$p_{max} = \frac{3\,F}{2\,\pi\,a^2}$$

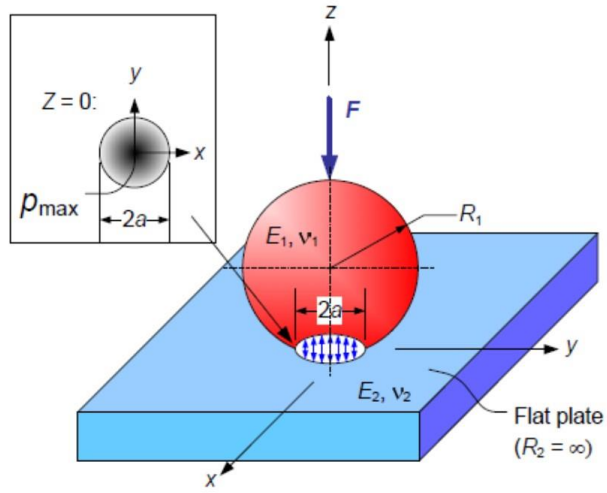

Figure 11: The method of maximum burst pressure calculations. A sphere on a flat plate (a flat plate is a sphere with an infinitely large radius). [65]

2.2.5 Multi-laminar Ply-Angle-Ply Patch Formation

Multi-laminar ply-angle-ply patches were formed in order to mimic the native AF architecture. Once the desired sheet orientation was achieved the necessary amount of layers could be tailored to the desired burst strength. In order to attach multiple sheets of

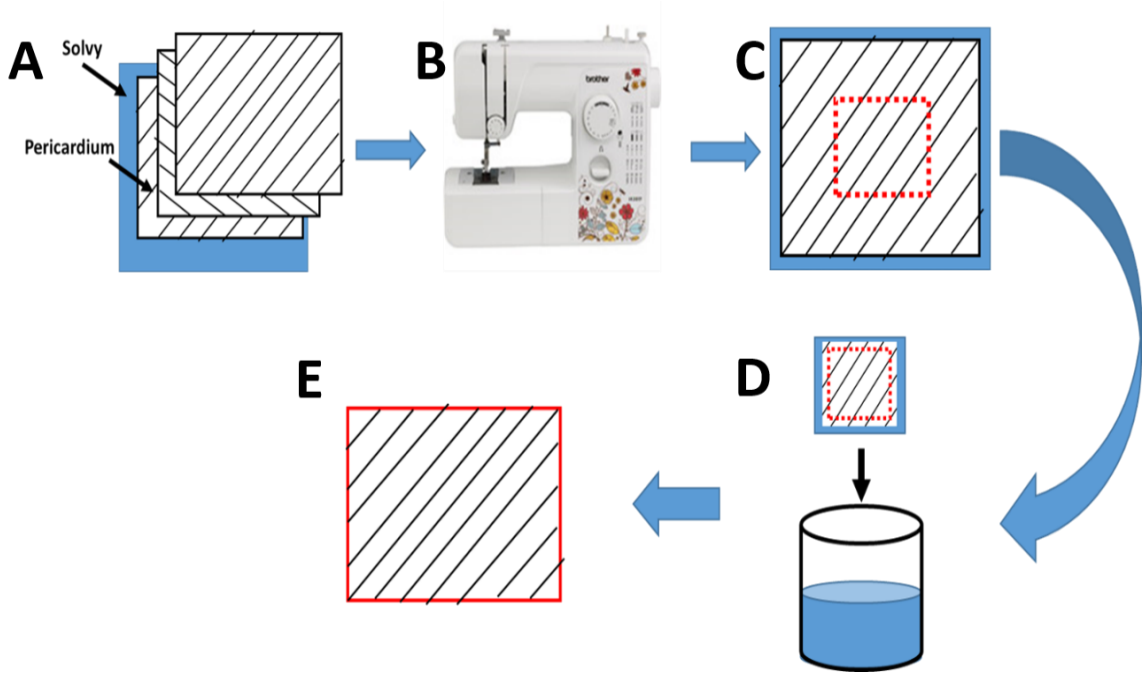

Figure 12: Representative diagram of the method for AF patch formation. A) The pericardium sheet fibers were aligned and placed on the tissue backing. B) The layers were then sewn with the sewing machine. C) A patch plus tissue backing was formed. D) The patch composite was then inserted into water to dissolve the tissue backing. E) Left was only the AF patch.

pericardium together to form a multi-laminate ply-angle-ply AF patch a standard sewing machine, tissue backing, and suture thread were used. The decellularized pericardium sheets were first gently dried with a kimtech wipe to remove excess moisture. The fiber preferred direction was then determined within each sheet using a light box. The sheets were then layered to create the ply-angle-ply orientation. The multiple layers were then set upon the tissue backing (fabric-solvy) for sewing in the sewing machine (**Figure 12**). The tissue backing was needed to allow the sewing needle to puncture all the layers of pericardium and to allow easier positioning of the layers in the sewing machine. A ~10 x 10 mm square was sewn into the layers to create the AF patch. The excess tissue backing

was then manually removed with tweezers and the excess tissue was trimmed away from the sutures with a scalpel blade. The patch was then added to a specimen cup of water for 30 minutes to ensure the degradation of any leftover tissue backing. This process was repeated to make multiple AF patches.

2.2.6 Bovine AF Cell Isolation & Culture

Bovine tails were collected at the time of slaughter from a local abattoir. The IVDs were dissected in half using mechanical shears. The NP was first removed in order to ensure harvest of only the AF. The AF tissue was then removed using scalpel blades and washed in a specimen cup containing 25 ml of sterile 2% antibiotic/antimitotic (Ab/Am) in phosphate-buffered saline (PBS). The tissue was then vortexed to ensure thorough washing. The tissue was then moved to the cell culture hood for manual mincing. The tissue was transferred using sterile tweezers to a sterile petri dish. The tissue was minced to between 2-4 mm using two scalpel blades and transferred to a 50 ml conical tube with 25 ml of collagenase solution (1% Ab/Am, 0.2% Collagenase Type I (125 units/mg dry weight) and DMEM). Tissue was digested overnight (~18 hours) at 37^{o}C with a loose lid. After digestion, the collagenase activity was stopped with pure FBS and gently mixed for 5-10 seconds. The digested solution was then passed through a sterile 100 µm cell strainer, and the flow through was collected into a new 50 ml conical tube. The solutions were then moved to a 15 ml conical tube for washing. The solution was centrifuged at 1000 rpms for 5 minutes. The supernatant was then removed and the cells were re-suspended in cell

culture media (1% Ab/Am, 10% FBS and DMEM). The cells were then counted and plated in a T175 at 3000-4000 cells/cm.^{2}

2.2.7 Suture Pull Out Strength of AF Patch

The suture pull out strength of the AF patch was determined using 6-0 prolene suture in a simple tensile test. The protocol method was developed from ASTM F2903 and previous company guidelines. The tensile testing was done using an MTS machine with a 100 N load cell. The suture was inserted 2 mm from the edge of the patch. The bottom edge of the patch was inserted into the bottom MTS clamp. The top ends of the suture was secured to the movable head of the machine, creating a loop of suture. The suture was then pulled to failure of either the suture or the patch at a rate of 75 mm/min.

2.2.8 Cytocompatibility of Multi-laminar Patches

Twenty-two 3-layer patches were prepared as described previously. In order for the patches to be used in the cytocompatibility study, the patches were re-sterilized. First, the patches were sterilized in a pee cup with 100 ml of 0.1% Peracetic Acid on a shaker at 150 rpms for 2 hours at room temperature. The patches were then washed in 100 ml of sterile PBS for 1 hour (3 solution changes) on a shaker at 150 rpms at room temperature. Next, the patches were neutralized in 100 ml of sterile 50% fetal bovine serum (FBS)/ 40% Dulbecco's Modified Eagle Medium (DMEM) + 1% antibiotic/antimitotic (Ab/Am) overnight on a shaker at 150 rpms at room temperature.

After sterilization, the patches were divided into multiple groups as shown in ***Figure 13***. Cultured bovine AF cells at passage 4 were seeded 1 x 10^6 cells in 75 µl of cell culture media onto the top of 16 patches then incubated at 37°C for 3 hours. Every 20 minutes the run off media was pipetted back on top of the patch. After incubation, the patches were then flipped using sterile tweezers and the same process was repeated for the other side of the patch. After another 2 and a half hours of incubation, the wells were filled with 2 ml of cell culture media. Three of the control patches did not receive cells, only cell culture media. A separate three patches received 2 million more cells. These cells were

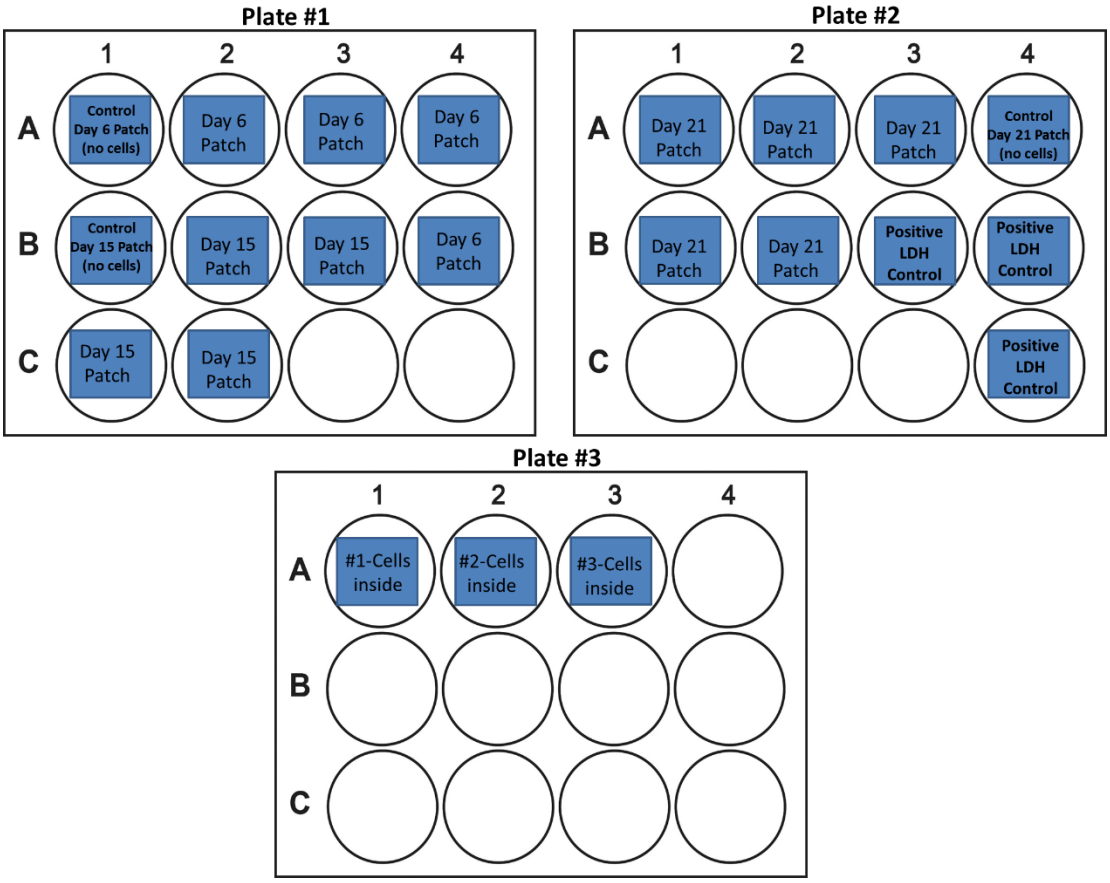

Figure 13: Cytocompatibility pilot cell study AF patch sample layout. Plate 1 – Day 6 and 15 patches. Plate 2 – Day 21 and positive LDH control patches. Plate 3 – patches with cells seeded inside and on top of them.

applied 1 million at a time to the inside layers of the patch with injection using a 27 gauge needle and syringe.

After cell seeding (day 0), the patches were analyzed at day 6, day 15, and day 21 with media changes every 3 days. The patches were moved to new 12 well plates with fresh cell culture media on day 3 to remove cells that did not attach to the patches. On day 3, the positive LDH control patches were frozen in liquid nitrogen for 1 min and thawed for 1 minute (repeated 3 times) to induce cell death. The patches were then put back in fresh media for 3 more days. On day 6, 8 patches were sacrificed. The media from all wells was removed and saved in labeled 2 ml centrifuge tubes for Lactase Dehydrogenase (LDH) analysis. The 8 patches were removed one at a time using sterile tweezers to a sterile petri dish. The control and 4 designated day 6 patches were each cut in half. Half of each patch were put into a labeled tissue cassette for histological analysis. The second half was then cut in half again. Each piece was then put into labeled 2 ml centrifuge tube for analysis. The whole positive LDH control patches were put into tissue cassettes for histological analysis. At day 15, 5 patches were sacrificed. The media was again removed from all wells and saved in labeled 2 ml centrifuge tubes for LDH analysis. The same removal and analysis process was used at each time point. At all time points, picogreen and LDH analysis were performed for the harvested patches to determine cell number and cell death, respectively. At day 15, hydroxyproline analysis was performed to determine collagen production.

A cell standard curve was made for picogreen to determine the amount of cells on each patch. The picogreen DNA cell standard curve was made by harvesting cells from 2D

culture using an appropriate detachment method. The cells were counted and re-suspended in duplicate in appropriate cell number ranges (4 million, 2 million, 1 million, 500,000, and 250,000 cells) in 1 ml lysis buffer (10 mM Tris pH8, 1mM EDTA, and 0.2% (v/v) Triton X-100). Cell samples were vortexed for 10 seconds every 5 minutes for half an hour, keeping on ice throughout. The cells were then homogenized 10-15 times using a 21-guage needle. Samples were the diluted to 1 in 10 with 90 µL of 1x TE Working Solution into the wells of a black bottom 96-well plate. 100 µL of the prepared PicoGreen Working Solution was then added to all wells and incubated at room temperature for 5 minutes wrapped in aluminum foil. The fluorescence was measured at excitations at 460 nm and emission at 540 nm, respectively resulting in a gradient of cellular DNA based on cell number. A similar process was used to determine DNA content on the AF patches. The patches were first washed in PBS and then placed in the 1 ml of lysis buffer. All the previous steps were then repeated.

A cell death standard was made using the positive LDH control patches as maximum cell death. 3 AF patches were seeded with 2 million cells (described previously) and cultured for 3 days in CCM. After 3 days, the cells were killed by submersion in liquid nitrogen and then returned to fresh CCM for 3 more days to allow for sufficient LDH production. The media was collected and measured for LDH in accordance with LDH protocol resulting in a 2 million cell positive cell death control.

2.2.9 Histological Analysis of Cell Seeded AF Patches

Representative samples were taken from corresponding studies, fixed in neutral buffered formalin for 24 hours, embedded with paraffin, and sectioned at 5 μm thickness. In order to visualize cellular material removal and tissue extracellular matrix, Hematoxylin and Eosin (H&E) staining was used. Qualitative alpha-gal removal was confirmed using immunohistochemistry (IHC) antibody Biotinylated Griffonia Simplicifolia Lectin I for xenoreactive alpha-gal epitope. The Axio Zeiss Vert. A1 camera microscopy with Axio vision SE64 Rel 4.9.1 software was using for imaging of slides.

2.2.10 Statistical Analysis

Results are represented as a mean ± the standard error of the mean (SEM). All statistical comparisons between two groups were performed by two-tailed student's t-test of unequal variance or ANOVA. Significant differences were defined as $p<0.05$.

CHAPTER 3

RESULTS

3.1 Decellularization of Porcine Pericardium

Decellularization of the pericardium was done to remove cells and cell debris (including DNA) and the porcine antigen alpha-Gal in order to reduce the potential for an immunological host response to the implanted constructs. The method of decellularization was modified and adapted from Tedder et al. More, specifically, the DNase/RNase concentration was modified after initial histological analysis showed small amounts of residual DNA. The concentration of DNase/RNase was doubled to ensure complete removal of all cellular DNA content. It was observed through histological H&E staining that cellular nuclei are distributed throughout the fresh porcine pericardium ECM. Images confirmed removal of all cell nuclei in the decellularized tissue sheets using this method (**Figure 14**). The remaining ECM was intact and exhibited some tissue swelling as was indicated by an increase in overall tissue thickness after the decellularization process.

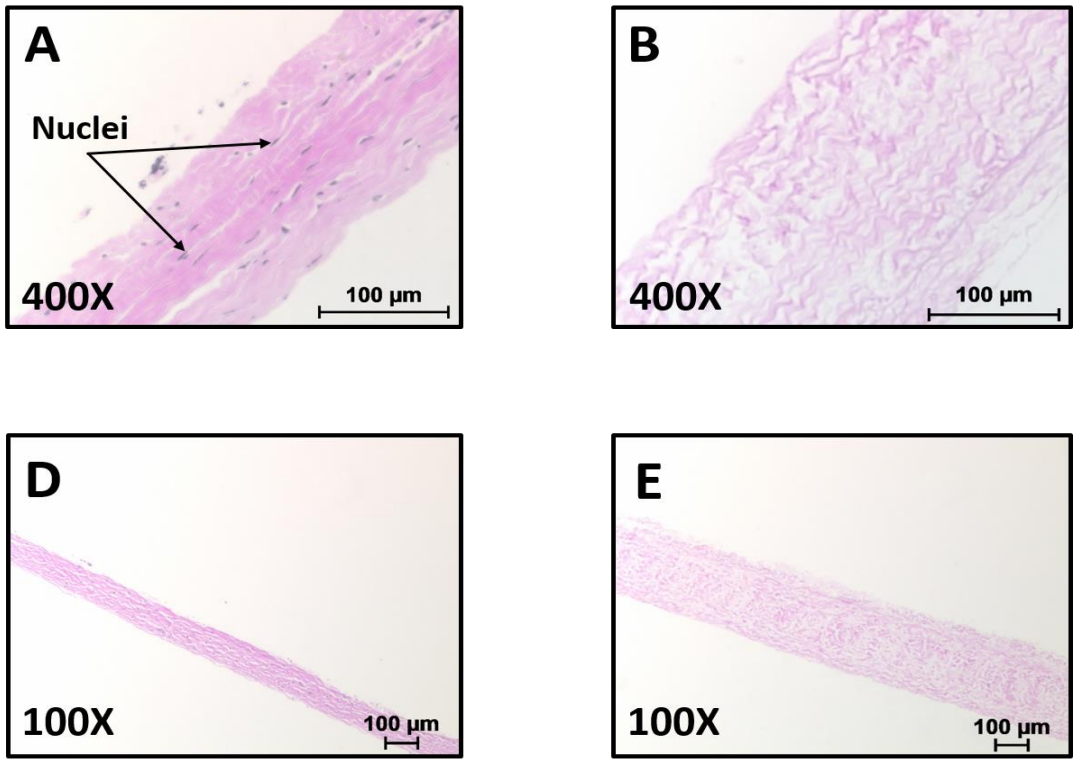

Figure 14: Representative H&E Images of porcine pericardium sheets. (A & D) Fresh tissue with cell nuclei (B&E) Decellularized tissue without cell nuclei [ECM – Pink, Cell Nuclei – Blue]

IHC for alpha-Gal confirmed the presence of the porcine antigenic epitope in fresh porcine pericardium tissue with positive staining (**Figure 15**) and its removal in the decellularized tissue as indicated by a complete lack of positive staining. These results suggest the successful removal of alpha-Gal through the modified decellularization process.

Agarose gel electrophoresis (**Figure *16***) and nanodrop quantification (**Figure 17**) results demonstrated significant reductions in cellular DNA content after decellularization ($p < .05$). The agarose gel clearly showed the presence of high molecular weight cellular DNA in the fresh porcine pericardium (as indicated by bright red bands) yet there was no detectible intact DNA or low molecular weight fragments in the decellularized tissue

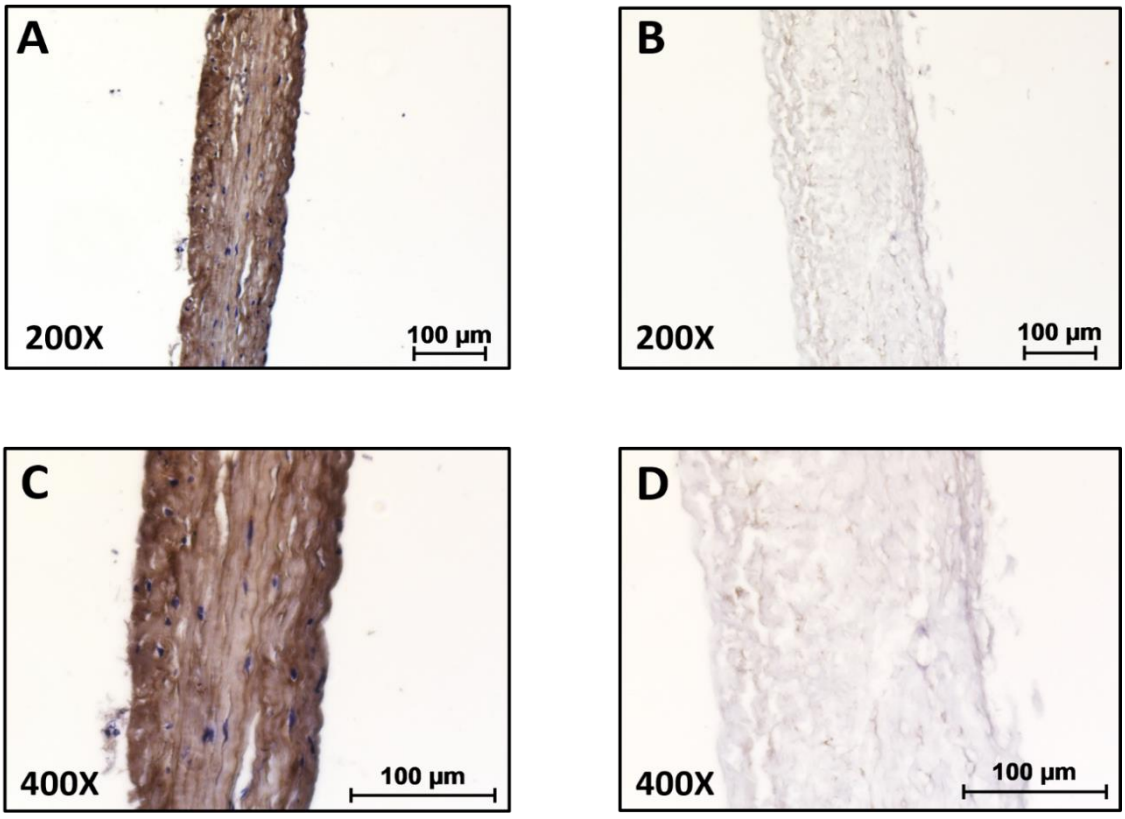

Figure 15: Representative images of IHC stain for alpha-Gal. (A&C) Fresh porcine pericardium (B&D) Decellularized porcine pericardium [Cellular Nuclei - Blue, Alpha-gal - Brown]

(**Figure *16***). Nanodrop results showed a 95.3% decrease in DNA from fresh to decellularized porcine pericardium. The decellularized and fresh tissue were found to have 96.2 ± 13.4 and 2051 ± 112.7 ng DNA per milligram of sample dry weight, respectively

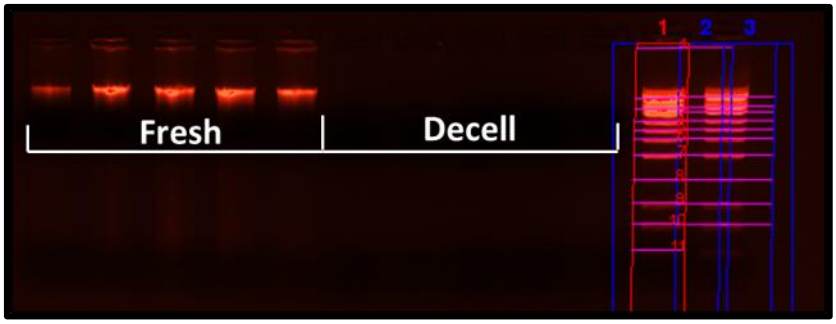

Figure 16: Agarose Gel Electrophoresis Results. (Left) DNA content bands for fresh and decellularized pericardium (Right) Standard DNA Ladder

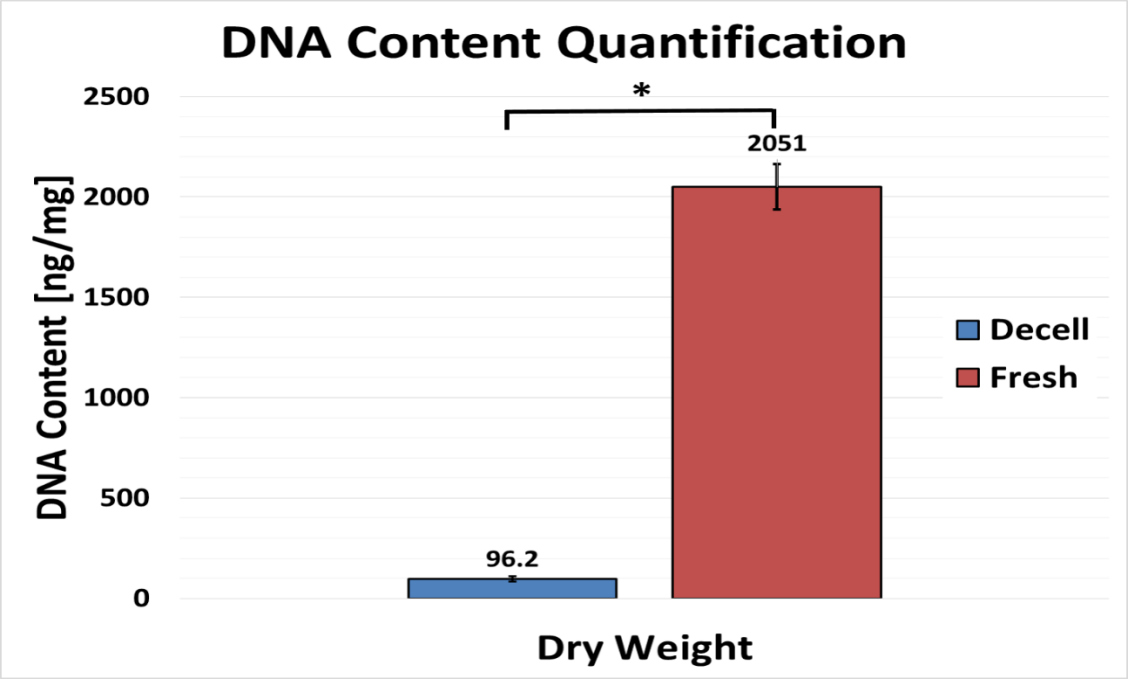

Figure 17: Quantification of cellular DNA content in fresh and decellularized porcine pericardium tissue. * indicates a significant difference ($p < 0.05$)

3.2 Decellularized Pericardial Tensile Strength

Uniaxial tensile testing in the fiber preferred and cross-fiber direction was performed on single sheets of fresh and decellularized porcine pericardium to ensure the tissue had similar mechanical properties to the native human AF. Tensile mechanical testing was performed on single-ply samples of pericardium to determine the tensile elastic modulus of the material and ensure the modified decellularization procedure did not alter the mechanical strength of the tissue. Tensile elastic modulus from 0.05 to 1.0 strain on the linear region of the stress strain curves were calculated so that direct comparisons to literature values could be made (**Figure 18**). Results indicated that the decellularization method had no significant effect on the tensile elastic modulus of the porcine pericardium (***Figure 19***) ($p < .05$). The cross fiber group had a slightly higher tensile elastic modulus with the fresh and decellularized tissue having 36.77 ± 6.4 and 27.16 ± 4.64 MPa, respectively. The fiber preferred group results again showed no significant difference between fresh and decellularized tissue groups which had 16.97 ± 3.9 and 20.59 ± 4.91 MPa, respectively. There was no statistically significant difference between the decellularized pericardium between the cross fiber and fiber preferred groups. The ultimate tensile strength (UTS) was also determined from the tensile testing and showed no significant difference between fresh and decellularized tissue groups in the cross fiber direction which had 4.53 ± .934 and 4.54 ± .803 MPa, respectively. Although, there was a significant difference found between the fresh and decellularized tissues UTS in the fiber preferred groups which had 7.99 ± 1.46 and 4.62 ± 0.702 MPa, respectively.

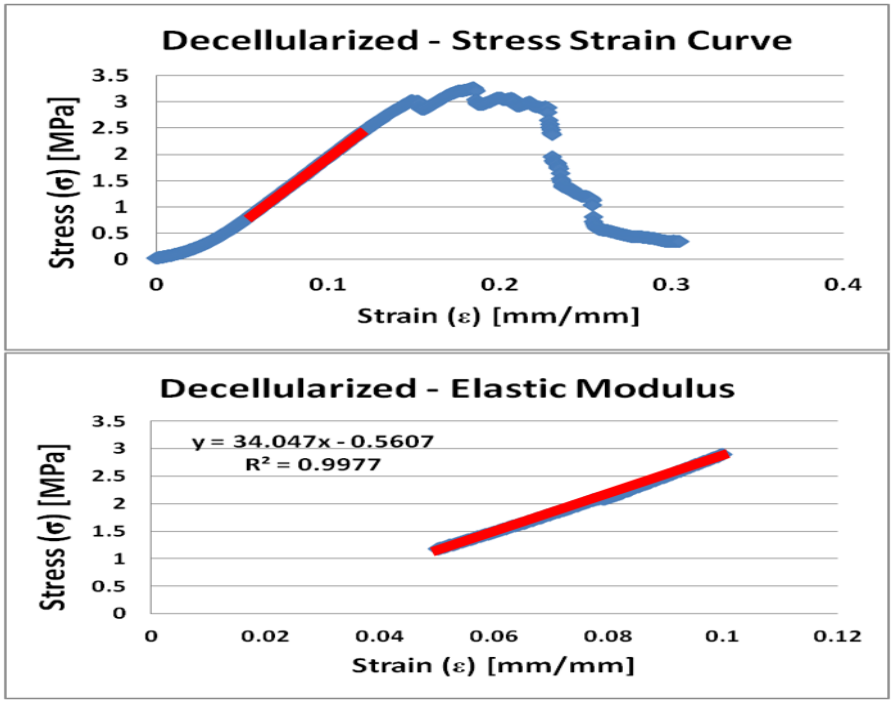

Figure 18: Representative stress strain curve of porcine pericardium tensile testing. (Top) Entire stress strain curve during tensile testing. (Bottom) Linear region of the stress strain curve from 0.05 to 1.0 strain.

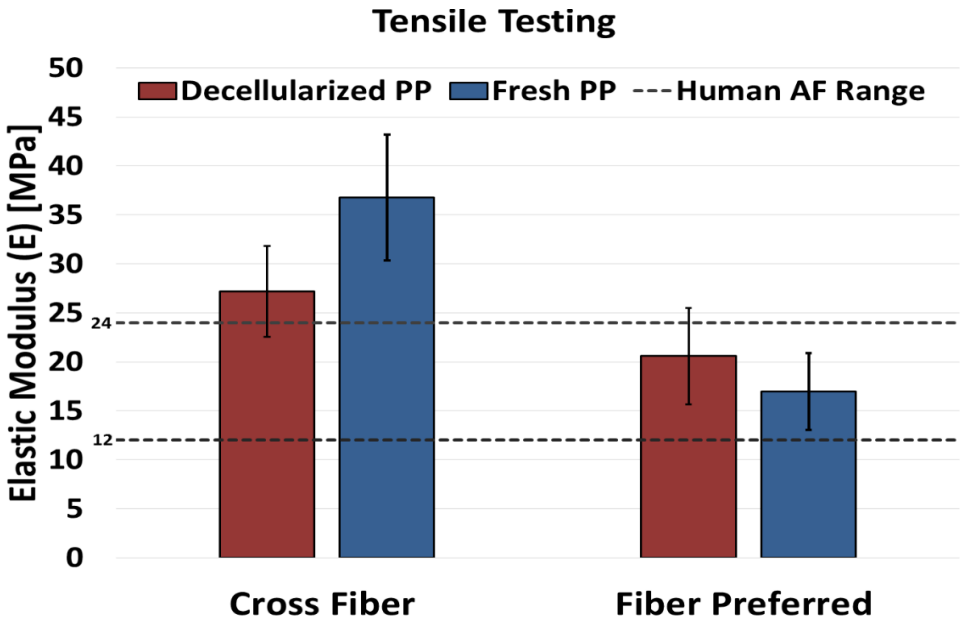

Figure 19: Average tensile elastic modulus of fresh and decellularized porcine pericardium samples. No significant difference was seen between fresh and decellularized tissue within each group ($p<0.05$).

3.3 Decellularized Pericardial Ball Burst Strength

Ball burst testing of multiple pericardium layers was performed to assess the maximum burst strength the pericardium could withstand and the necessary number of layers needed to resist the IDP generated by the NP exerted on the AF as a hoop stress. The burst strength of the pericardium layers was calculated using the peak load each group could withstand before bursting. These peak loads were taken from the load/extension graphs made for each sample tested (**Figure 20**). The burst strength of the groups showed the strength increased significantly with the number of layers used (**Figure 20**). 1, 2, 3, and 6 layers all exceeded the internal IVD IDP of 2.3 MPa with 4.26 ± .40, 7.53 ± .52, 10.75 ± 1.47, and 18.49 ± .76 MPa, respectively. Statistical analysis performed with ANOVA showed all test groups were significantly different from all other test groups ($p<0.05$).

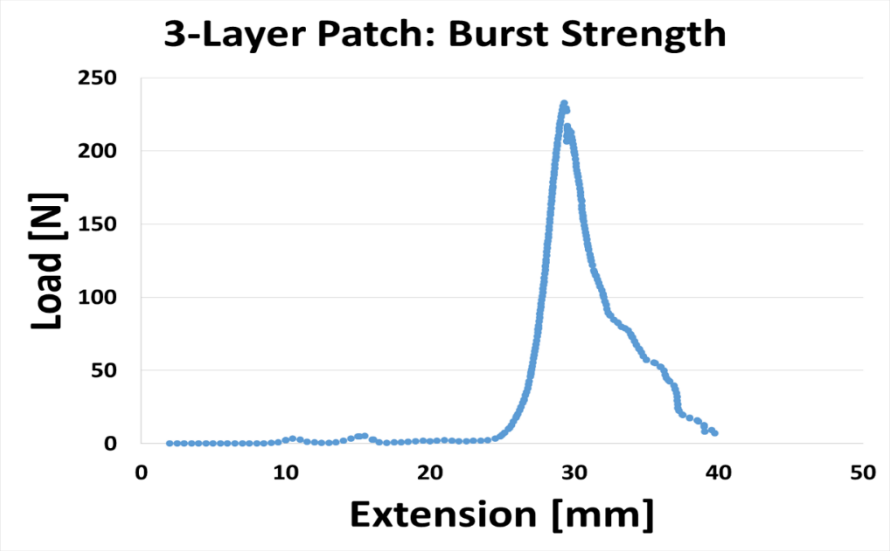

Figure 20: Representative image of the load needed to burst a 3-layer AF patch.

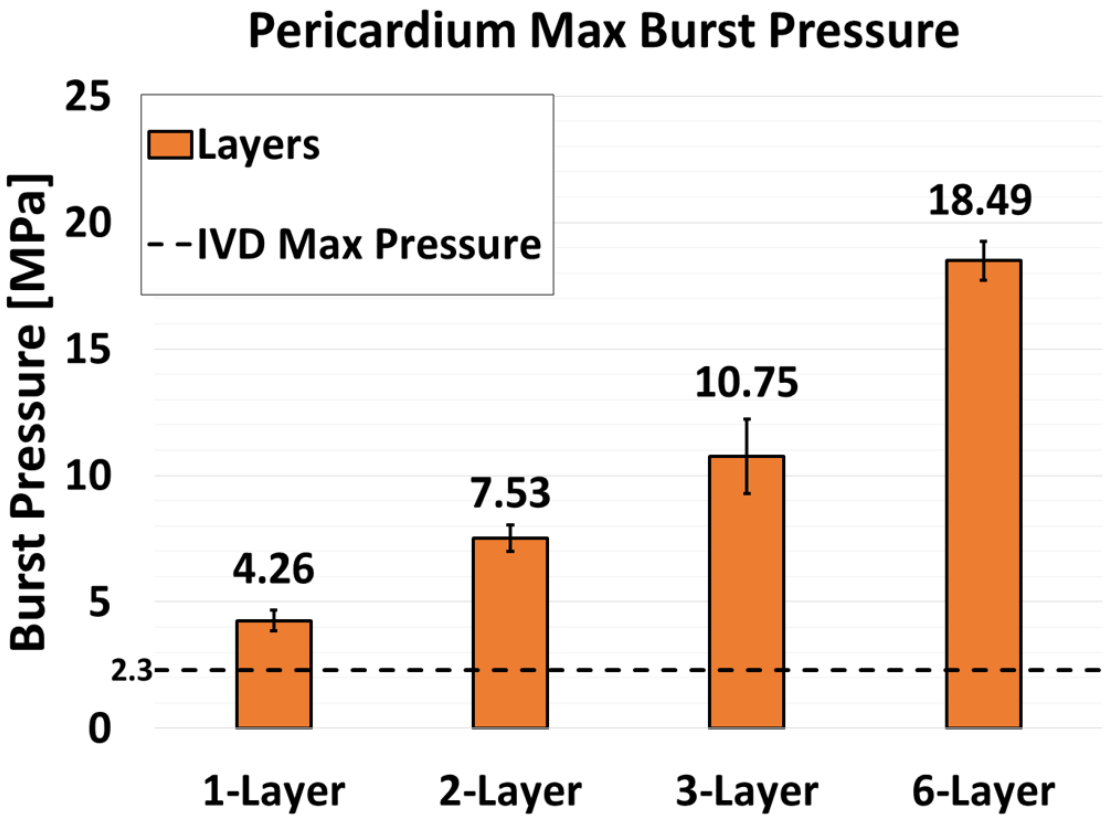

Figure 21: The maximum calculated burst pressure 1, 2, 3, and 6 layers of pericardium can withstand.

3.4 AF Patch Formation

The AF patch formation method went through many different iterations in order to succeed in the finalized AF patch formation methodology. Many methods required a significant amount of tissue to form one small patch which limited the amount of patches that could be made. A tissue backing was also required in order grip the material during sewing. The pericardium tended to be slippery and difficult to hold in alignment without the backing. The backing also provided enough stiffness for the needle to successfully penetrate all layers. Initial patch formation was using a stiff fabric backing that was simple to sew but proved to be difficult to remove without disrupting the AF patch. The next method was using a kimtech wipe as tissue backing given it would tear easily from the back of the tissue. This again proved to be unsuccessful due to residual kimtech wipe being difficult to remove from beneath the tissue sutures. The patches needed to be sterilized and leftover backing material would render that process ineffective. The final method was

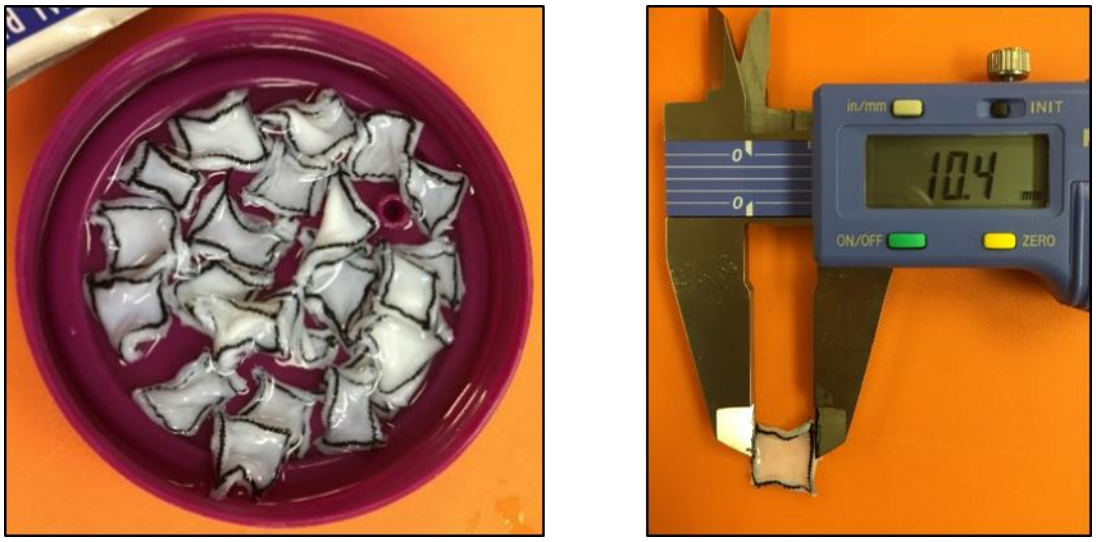

Figure 22: (Left) Representative 22 3-layer AF patches in a specimen lid. (Right) One 3-layer AF patch 10.4 mm in width.

decided upon due to fabric-solvy's fabric like feeling and dissolvability in water. This method also allowed for smaller tissue to be used in order to conserve available pericardium. Successful sewing of twenty-two 3-layer AF patches was done using the finalized method (**Figure 22**). All 3-layered AF patches were ~ 8-12 mm with all of them less than 1 mm thick.

The layers within the AF patches were specifically oriented during patch formation to mimic the native AF ply-angle-ply architecture. Histological analysis of the 3-layered AF patches showed the fiber orientation between each layer was difficult to determine even though, each individual layer of the patch could easily be identified.

Suture pullout strength was investigated to ensure suitable strength of the AF patch material to be fixed to the native tissue during implementation of the AF patch. The testing results showed the 6-0 prolene suture failed at the point of contact with the patch before any failure of the patch was evident. The average suture failure strength was measure to be 7.05 ± 1.23 N.

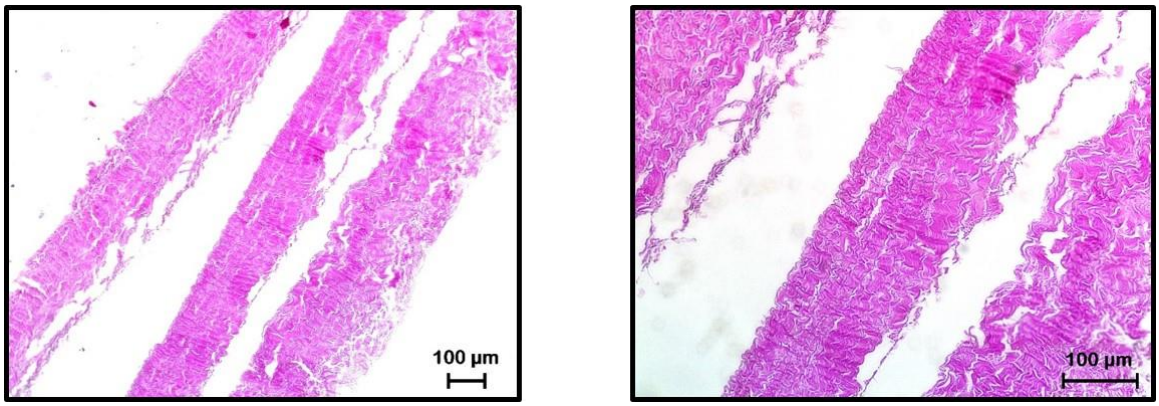

Figure 23: Representative H&E images of a 3-layer AF patch and fiber alignment.

3.5 AF Patch Cytocompatibility

To determine the cytocompatibility of the AF patches, the patches were seeded with bovine AF cells and cultured for 15 days *in vitro*. Histological images at day 6 and 15 time

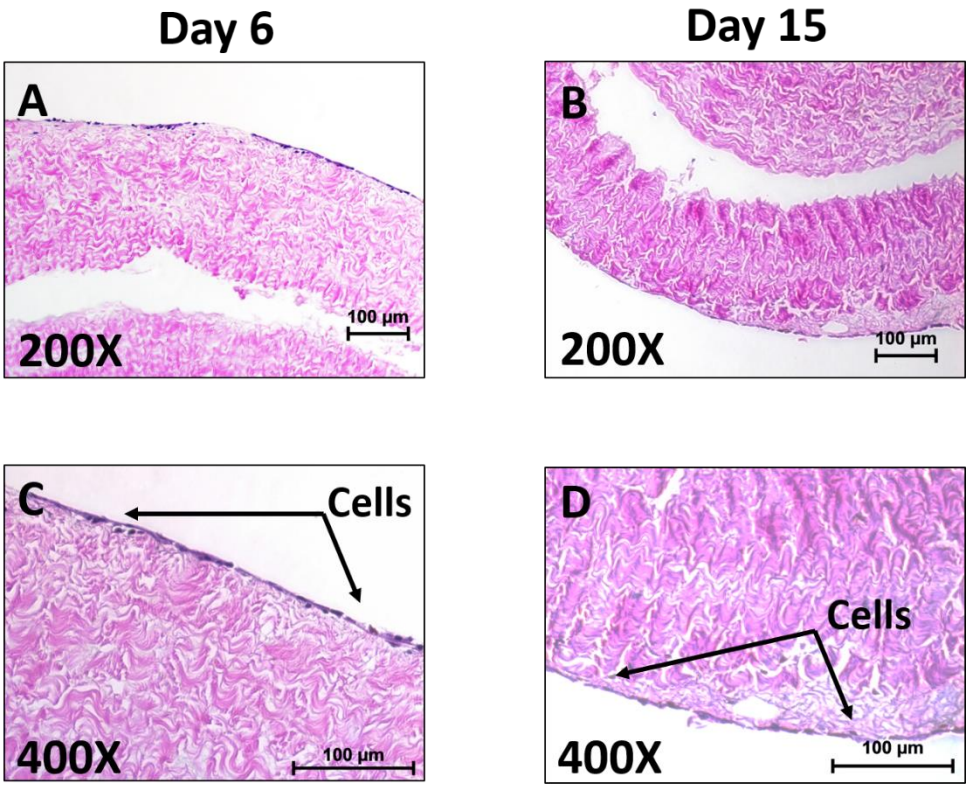

Figure 24: Representative images of the 3-layer AF patches after 6 and 15 days in cell culture. Cells can be seen on the surface of the patches. (A&C) Day 6 patch images (B&D) Day 15 patch images [Pink-ECM, Blue-Nuclei]

points showed a layer of cells on the outermost layer of the cultured patches (**Figure 24**). No cellular migration into the AF patches was seen. Histology also showed no cells inside specific patches even though the cells were manually seeded in between the layers. It was also noted that there was a higher density of cells seen on the top surface of the patch than on the bottom layer (facing the bottom of the well plate) of the patch.

To determine cytocompatibility the amount of cell death and proliferation was determined. The amount of LDH released into cell culture media by dead cells did not increase over the course of the study, indicating the cell death did not progress. The results showed only an 18.4 and 19.6% release of LDH at day 6 and day 15, respectively (**Figure 25**), which were not significantly different.

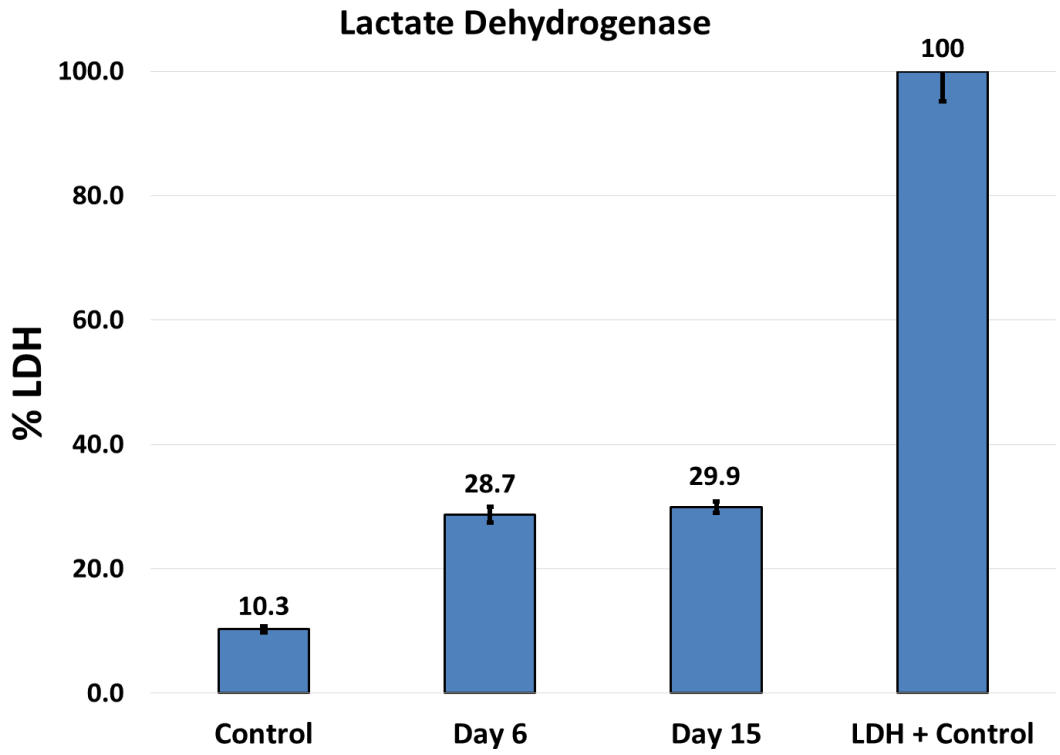

Figure 25: The amount of lactate dehydrogenase produced at day 6 and day 15. The control did not have any seeded cells. The LDH positive (+) control was 100 % cell death of the seeded cells after attachment.

The amount of DNA content on the cultured AF patches was determined using PicoGreen analysis of a representative portion of the AF patch at day 6 and 15. DNA content is directly related to the amount of cells on the AF patches which could be approximated based on cell standards. The amount of DNA in 250,000 and 500,000 cell was used to interpret the amount of cells found on the patches at day 6 and 15 (**Figure 26**). There was no statistical increase found between day 6 and 15 but the data trended towards an increase in DNA on day 15. The amount of DNA found at day 6 and day 15 were 0.264 ± .081 and 0.361 ± .074 µg of DNA per ml, respectively. Taken together with the LDH findings, it does not appear that the material induces an increase in cell death overtime thus illustrating cytocompatibility.

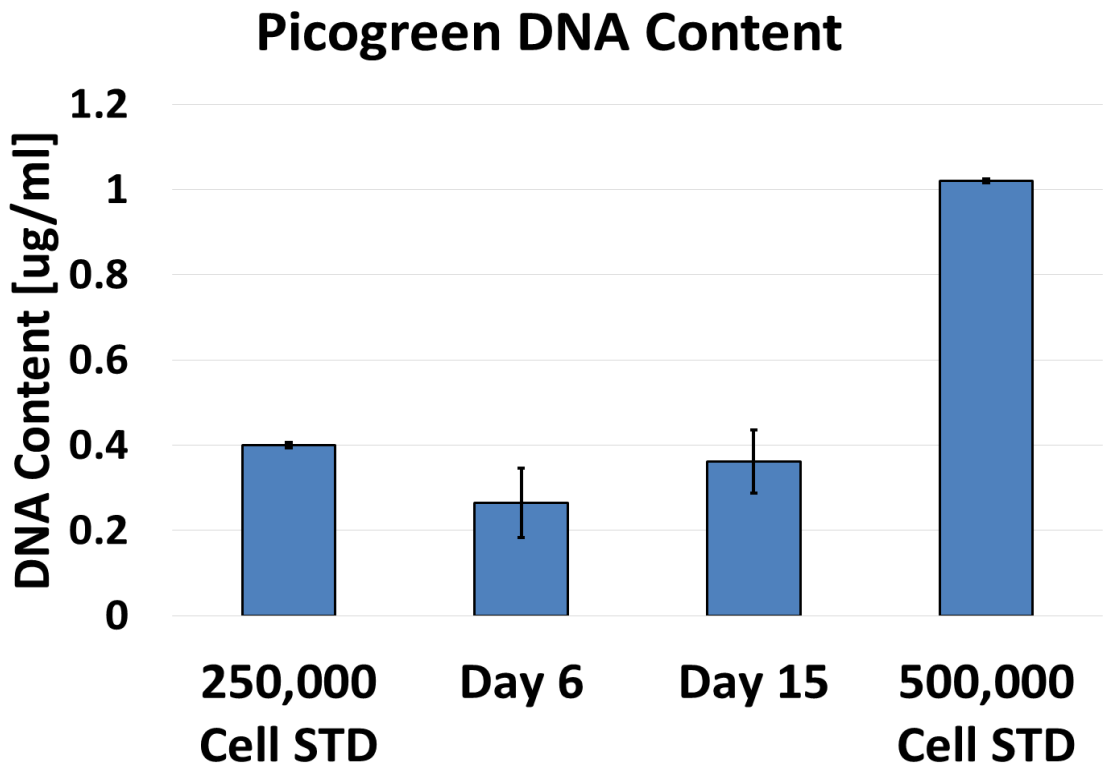

Figure 26: The amount of DNA content on the cultured AF patches at day 6 and 15 using picogreen analysis. The 250,000 and 500,000 represent the DNA cell standards of 250,000 and 500,000 cells, respectively.

CHAPTER 4

DISCUSSION

4.1 Decellularization of Porcine Pericardium

When performing tissue decellularization for biomimetic scaffold development, a balance must be met between achieving complete decellularization and the preservation of the ECM for biomechanical stability and function. The immunogenicity of acellular matrixes must be eliminated before they are used for tissue engineering. Cells are the main immunogenic factor due to histocompatibility antigens distributed on the surface of cell membranes. Histocompatibility antigens are recognized by T cells, and the tissue is attacked by the host after transplantation. So, before porcine pericardium is used as a scaffold the cells were removed to avoid immune rejection and inflammation. The H&E images showed that the modified decellularization protocol successfully removed the cellular DNA fragments and the xenoreactive antigen in porcine tissue, alpha-Gal. These findings were confirmed in the agarose gel electrophoresis which also did not detect any DNA. A small amount of DNA, <100 ng/mg dry weight of tissue, was quantified in the decellularized tissue using nanodrop. These results are in alignment with previous results showed by Tedder et al. when using a similar decellularization protocol.[46] While there has been recent research into the amount of DNA that will illicit an intense immune response, an exact 'threshold' has not yet been determined.[53] It is well known that a decreased amount of cellular 'debris' correlates to a decrease in immune response and by reducing the DNA content by 95% this scaffold should not illicit a significant host immune response. Keane

et al. clearly showed that an increase in DNA fragment size is associated with a more pro-inflammatory macrophage phenotype and based on the agarose gel decellularization results the AF patch contains only low molecular weight DNA.

4.2 Decellularized Porcine Pericardium Mechanical Properties

Following decellularization, it was important to determine the effects on the biomechanical properties of the decellularized scaffold. The tensile mechanical testing of the pericardium showed that the decellularization process did not significantly alter the tensile elastic modulus of the tissue since there was no statistical significance seen between the fresh and decellularized tissue within each group. The determined tensile elastic modulus of the decellularized tissue was also comparable to values reported for human AF in literature.[54] The main distribution of forces throughout the AF are in tension during bending or twisting on the spinal unit. Furthermore, AF layers have to resist hoop stresses developed due to the IDP of the NP. As such, the AF patch should attempt to re-establish this key native property. The decelled porcine pericardium tensile elastic modulus in cross fiber and fiber preferred directions were 27.16 ± 4.64 and 20.59 ± 4.91 MPa, respectively. A single lamellae of human AF tissue has a tensile elastic modulus range reported between 12 and 24 MPa.[48] Variations in testing methods and sample size and directions may have contributed to the slightly higher value in the cross fiber direction. Also, no statistical significance was found between the decellularized tissue in the cross fiber and fiber preferred groups. This could be due to the pericardium sheets having strong underlying cross-linked fibers in the cross fiber direction resulting in the pericardium having a higher

tensile elastic modulus in the cross fiber directions. These cross-linked fibers are suspected to be stiffer but have a lower UTS. This was verified when the fiber preferred fresh pericardium had a significant higher UTS when compared to decellularized pericardium. The fiber preferred tissue has a lower tensile elastic modulus due to the collagen fibers having an initially crimped structure that stretches out before providing resistance in tension. The collagen fibers are less stiff than the cross-linking fibers in the fiber preferred direction resulting in a lower tensile elastic modulus but they can resist a larger load, resulting in a higher UTS.

The ball burst mechanical testing was deemed necessary to investigate the multi-axial burst strength of the decellularized pericardium. When the spinal unit is under compression the NP exerts an IDP radially out onto the AF generating a tensile hoop stress which impart is responsible for keeping the NP contained inside the IVD and adding stability to the functional spinal unit.[32] The pericardium needs to be able to withstand this pressure from the NP in order to prevent expulsion of the NP. Testing was performed on 1, 2, 3, and 6 layers of pericardium in order to determine the appropriate number of layers needed to adequately withstand the NP's IDP. The highest reported IDP inside the NP of a human volunteer was 2.3 MPa while picking up a 20 kg object.[55] After each addition of a pericardial sheet, a significant increase in burst strength was seen. The burst testing showed that one layer of pericardium could potentially withstand the NP IDP (4.26 MPa) but in order to incorporate a significant safety factor; 3 layers of pericardium may be beneficial (10.75 MPa).

4.3 AF Patch Formation

Once the adequate number of layers to resist the NP burst pressure was determined 3-layered AF patches could be developed. The AF patch formation method was vital in mimicking the native AF tissue architecture. This native ply-angle-ply multi-laminate architecture is responsible for distributing tensile bending and torsional forces throughout the functional spine unit.[56] By manually alternating the fiber preferred direction of the pericardial tissue sheets, the ply-angle-ply orientation was developed. The sheets of pericardium were then fixed in the determined orientation through sewing of the layers together on a tissue backing. This tissue backing made the sewing method possible and was ideal due to its complete dissolution in water. After the AF patch was sewn together it was placed in water to dissolve off the tissue backing. This process allowed for no residual to be leftover behind the suture and for the patch to be sterilized using a neutral pH peracetic acid solution. The developed method of AF patch formation can be more readily scaled for manufacturing methodologies compared to other AF TE methods.[40,57]

The confirmation of the 3-layered AF patches ply-angle-ply architecture was difficult to demonstrated though histological images. We believe this is due to the patches being sectioned on end and the fiber alignment being presented perpendicular to the view. Polarized light was used to try and refracted the light based on the fiber orientation within each layer of pericardium. This was predicted to result in a color alteration between the individual layers. The images however did not present this color change. Even though macroscopically the fiber orientation can be determined the method of histologically imaging the fiber orientation needs to be developed further.

After making the AF patches the suture pull-out strength needed to be determined to ensure the mechanical strength of the patch to be sutured to the native AF tissue. The suture pull-out test is vital for a TE material because the suture automatically creates a puncture defect in the material where the stress will now increase at. The suture most commonly used in spine surgery, 6-0 prolene, was used for testing. The testing results supported that the AF patch has sufficient suture pull out strength given that the sutures failed before the patch showed initial signs of failure.

4.4 Cytocompatibility of AF Patch

In conjunction with the use of scaffolds, AF TE requires the use of cells which have the capacity to regenerate the ECM by maintaining the long-term homeostatic balance of matrix turnover. The AF patch needs to be cytocompatible with these cells in order for it to be integrated into the native host tissue. It's our goal to make a construct that can eventually integrate with the host tissue by allowing for infiltration of viable host AF cells. This was tested through the seeding of bovine AF cell on the multi-laminate AF patches. Human AF cells were not used due to the unavailability of human IVD's that are not damaged or degenerated. There is little feasibility in using healthy human native AF cells since its harvest is destructive to the whole IVD. The bovine AF cells were used to test cytocompatibility of the AF patch with cells with an end-stage phenotype found in the native AF. Histological H&E images showed that the multi-laminate AF patch was cytocompatible. Cells were seen in a uniform layer across the top outermost layer of the AF patch at day 6 and 15. A lower cell density was seen on the bottom layer of the patch

(facing the bottom of the cell culture well), suggesting that a longer resting time may be needed before the patch is flipped to seed the other side to improve the amount of attached cells. Since some cells were seeded on the inside patch layers, but cellular material was only seen on the outermost layers, the cells on the inner layers of the patch may have died and detached before histological images could be taken. This could have been due to the dense ECM of the pericardium made it difficult for the cells to receive nutrients through the layers of the patch. This could potentially be improved if pores could be created in the patch layers for nutrient exchange. The cells undergo a natural rate of proliferation and apoptosis which can be seen in the LDH and DNA content data. LDH is a cytosolic enzyme that is released into the media from damage and acts as an indicator of cellular cytotoxicity. The media is changed every three days so at day 6 and day 15 there is only 3 days' worth of LDH released into the media. Since the results showed no increase in LDH release (~19%) for three days we can conclude the AF patch is not cytotoxic to the cells otherwise we would likely observe a much higher percentage of LDH released to the media. The amount of cells on the patches was determined using DNA content. Day 6 results showed less than 250,000 were adhered to the patch. This is relatively low given the initial seeding density, suggesting that the cell seeding method needs to be optimized. Although no significant increase in the amount of cellular DNA between Day 6 and 15 was seen there was a trend towards an increase in cell numbers on Day 15. This could be due to the low number of cells that initially adhered to the patch, possibly an effect of too high of a media volume used during seeding. While the use of AF cells allow for studying the effect of the AF patch scaffold on cell behavior, the need for an alternative to AF cells arises in clinics

due to the fact that xenogeneic cells are not a viable option and invasive surgical procedures are required for AF cell isolation. MSCs could be an alternative for this application as they are readily available from bone marrow or adipose tissue. However, research is still unclear of the specific markers that direct stem cells to a discogeneic phenotype. The data of the present study in terms of AF cell cytocompatibility shows that the cells can adhere to the scaffold and remain viable for an extended period of time.

While cells were seeded in between the layers of 3 of the AF patch, results would suggest they did not survive inside the patch. Histological H&E images did not show any attached cellular material between the layers of the patch. This is most likely due to the lack of oxygen and nutrient exchange inside the patch. The AF patches ECM is very dense and nonporous and the sewn edges make them almost water tight. This could potentially be solved by creating pores in the outer layers of the AF patch to allow for nutrient exchange.

CHAPTER 5

CONCLUSIONS & RECOMMENDATIONS FOR FUTURE STUDIES

5.1 Conclusions

Over the last few years there has been a significant push to develop AF TE devices to create an early-stage treatment option for patients with IVDD or IVDH. Potential scaffolds have continued to fall short when either mimicking the native AF ply-angle-ply architecture or creating mechanically stable constructs. However, we have illustrated the ability to repeatedly manufacture a unique ply-angle-ply multi-laminate AF patch which could be used to create an intact AF. The AF patch contains suitable tensile elastic modulus and burst strength to withstand daily spinal motion and pressures. It has also proven to be cytocompatible with native AF cells and support cell viability. The multi-laminate AF patch could be used in adjust with an NP replacement for IVDD or after discectomy to help mitigate the risk of re-herniation. Further investigation into the attachment of the AF patch to the native tissue needs to be carried out. Only then will we begin to establish the exact method of implementation of this device.

5.2 Recommendations for Future Studies

The next logical step for future studies would be to perform a cellular study using MSC's to determine if they would be a viable options for implementation onto the AF patch. Testing would need to be done to determine the cell's differentiation capacity towards an AF cell-like phenotype on the patch. It would also be a great study to perform a long-term implantation of the AF patch to determine the response *in vivo* in the native

environment of the IVD. Cellular response could be investigated for biocompatibility and integration into the native tissue. It could also be key to develop a method to seed cells successfully to the inside of the patch. The pericardium ECM is naturally too dense for cellular migration through it but perforating the material could be a viable option if mechanical stability is not sacrificed. Another key component of the native AF is GAG content, while not as high as in the NP, it still plays a significant role in reducing friction between the AF sheets. If GAG could be incorporated between the layers of the patch its long term mechanical stability under spinal motion could potentially be preserved.

The order of importance in the future work should be taken into consideration as follows:

1. Determine a method for creating pores in the pericardium and determine the effect on the mechanical properties of the tissue
2. Perform another cell viability study on the inner layers of the patch after successfully creating pores
3. Perform a cell differentiation study with MSCs on the patch
4. Incorporate GAG between the layers and determine the effect on the patch's mechanical properties

REFERENCES

1. Jensen M, Brant-Zawadzki M. Magnetic Resonance Imaging of the Lumbar Spine In People Without Back Pain. 1994.

2. Vallfors B. Acute, subacute and chronic low back pain: clinical symptoms, absenteeism and working environment . *Scand J Rehabil Med*. 1985.

3. In Project Briefs: Back Pain Patient Outcomes Assessment Team (BOAT). *MeEDTEP*. 1(1).

4. Guterl CC, See EY, Blanquer SBG, et al. Challenges and strategies in the repair of ruptured annulus fibrosus. *Eur Cell Mater*. 2013;25:1-21. http://www.pubmedcentral.nih.gov/articlerender.fcgi?artid=3655691&tool=pmcentrez&rendertype=abstract.

5. Boden SD, McCowin PR, Davis DO, Dina TS, Mark a S, Wiesel S. Abnormal magnetic-resonance scans of the cervical spine in asymptomatic subjects. A prospective investigation. *J Bone Joint Surg Am*. 1990;72:1178-1184.

6. Schoenfeld AJ, Weiner BK. Treatment of lumbar disc herniation: Evidence-based practice. *Int J Gen Med*. 2010;3:209-214. http://www.pubmedcentral.nih.gov/articlerender.fcgi?artid=2915533&tool=pmcentrez&rendertype=abstract. Accessed March 18, 2015.

7. Keskimaki. Reoperation after lumbar disc surgery: A population based study of regional and interspecialty variations. 2000.

8. Malter. 5-year reoperation rate after different types of lumbar spine surgery. 1998.

9. Yorimitsu E, Chiba K, Toyama Y, Hirabayashi K. Long-Term Outcomes of Standard Discectomy for Lumbar Disc Herniation. *Spine (Phila Pa 1976)*. 2001;26(6):652-657. doi:10.1097/00007632-200103150-00019.

10. Carragee EJ, Spinnickie AO, Alamin TF, Paragioudakis S. A prospective controlled study of limited versus subtotal posterior discectomy: short-term outcomes in patients with herniated lumbar intervertebral discs and large posterior anular defect. *Spine (Phila Pa 1976)*. 2006;31(6):653-657. doi:10.1097/01.brs.0000203714.76250.68.

11. Miller JAA, Schmatz C. Lumbar disc degeneration: correlation with age, sex and spine level in 600 autopsy specimens. 1988.

12. GlobalData. 2013. http://www.globaldata.com/. Accessed February 4, 2015.

13. Agency for Healthcare Research and Quality. http://www.ahrq.gov/. Accessed February 4, 2015.

14. Hilibrand AS, Robbins M. Adjacent segment degeneration and adjacent segment disease: The consequences of spinal fusion? *Spine J*. 2004;4:190-194. doi:10.1016/j.spinee.2004.07.007.

15. Urban JPG, Roberts S. Degeneration of the intervertebral disc. *Arthritis Res Ther*. 2003;5(3):120-130. doi:10.1186/ar629.

16. Schnuerer A, Gallego J, Manuel C. *Core Curriculum for Basic Spinal Trianing*. 3rd ed.; 2005.

17. Urban. The nucleus of the IVD for Development to Degeneration. 2000.

18. Adams M a, McNally DS, Dolan P. "Stress" distributions inside intervertebral discs. The effects of age and degeneration. *J Bone Joint Surg Br*. 1996;78(6):965-972.

19. Fosang TEHAJ. Proteoglycans: many forms and many functions. *The FASEB*. 1992;6. http://www.fasebj.org.libproxy.clemson.edu/content/6/3/861.full.pdf. Accessed March 18, 2015.

20. Kluba T, Neimeyer T, Gasissmaier C. Human Anulus Fibrosis and Nucleus Pulposus Cells of the Intervertebral Disc: Effect of Degeneration and Culture System on Cell Phenotype. *Spine (Phila Pa 1976)*. 2005;30(24). http://journals.lww.com/spinejournal/Abstract/2005/12150/Human_Anulus_Fibrosis_and_Nucleus_Pulposus_Cells.7.aspx. Accessed March 18, 2015.

21. Schollmeier G, Lahr-Eigen R, Lewandrowski KU. Observations on fiber-forming collagens in the anulus fibrosus. *Spine (Phila Pa 1976)*. 2000;25(21):2736-2741. doi:10.1097/00007632-200011010-00004.

22. Bron JL, Helder MN, Meisel HJ, Van Royen BJ, Smit TH. Repair, regenerative and supportive therapies of the annulus fibrosus: achievements and challenges. *Eur Spine J*. 2009;18(3):301-313. doi:10.1007/s00586-008-0856-x.

23. Raj PP. Intervertebral disc: Anatomy-physiology-pathophysiology-treatment. *Pain Pract*. 2008;8(1):18-44. doi:10.1111/j.1533-2500.2007.00171.x.

24. Wilke H-J, Ressel L, Heuer F, Graf N, Rath S. Can prevention of a reherniation be investigated? Establishment of a herniation model and experiments with an anular

closure device. *Spine (Phila Pa 1976)*. 2013;38(10):E587-E593. doi:10.1097/BRS.0b013e31828ca4bc.

25. Carragee EJ, Han MY, Suen PW, Kim D. Clinical outcomes after lumbar discectomy for sciatica: the effects of fragment type and anular competence. *J Bone Joint Surg Am*. 2003;85-A:102-108.

26. Hughes T. The pathogenesis of degeneration of the intervertebral disc and emerging therapies in the management of back pain. 2012. doi:10.1302/0301-620x.94b10.

27. Adams M a. Biomechanics of back pain. *Acupunct Med*. 2004;22(4):178-188. doi:10.1136/aim.22.4.178.

28. WebMD - Back Pain. 2005. http://www.webmd.com/back-pain/guide/sciatica-pain-relief-options?page=2. Accessed March 4, 2015.

29. Lequin MB, Barth M, Thom C, Bouma GJ. Primary Limited Lumbar Discectomy with an Annulus Closure Device : One-Year Clinical and Radiographic Results from a Prospective , Multi-Center Study. 2012;9(4):340-347.

30. Dunlop RB, Adams M a, Hutton WC. Disc space narrowing and the lumbar facet joints. *J Bone Joint Surg Br*. 1984;66(5):706-710.

31. Eisner W. The Anulex Wrning. 2011.

32. Chiang YF, Chiang CJ, Yang CH, et al. Retaining intradiscal pressure after annulotomy by different annular suture techniques, and their biomechanical evaluations. *Clin Biomech (Bristol, Avon)*. 2012;27(3):241-248. doi:10.1016/j.clinbiomech.2011.09.008.

33. Optimizing discectomy outcomes in high-risk patients: Barricaid Prosthesis for Parial Anulus Replacement. 2014.

34. Kandel R, Roberts S, Urban JPG. Tissue engineering and the intervertebral disc: The challenges. *Eur Spine J*. 2008;17(SUPPL. 4):480-491. doi:10.1007/s00586-008-0746-2.

35. Bron JL, van der Veen AJ, Helder MN, van Royen BJ, Smit TH. Biomechanical and in vivo evaluation of experimental closure devices of the annulus fibrosus designed for a goat nucleus replacement model. *Eur Spine J*. 2010;19(8):1347-1355. doi:10.1007/s00586-010-1384-z.

36. Helen W, Merry CL, Blaker JJ, Gough JE. Three-dimensional culture of annulus fibrosus cells within PDLLA/Bioglass composite foam scaffolds: assessment of cell attachment, proliferation and extracellular matrix production. *Biomaterials*. 2007;28(11):2010-2020. doi:10.1016/j.biomaterials.2007.01.011.

37. Chan BP, Leong KW. Scaffolding in tissue engineering: general approaches and tissue-specific considerations. *Eur Spine J*. 2008;17 Suppl 4:467-479. doi:10.1007/s00586-008-0745-3.

38. Leung VYL, Chan D, Cheung KMC. Regeneration of intervertebral disc by mesenchymal stem cells: Potentials, limitations, and future direction. *Eur Spine J*. 2006;15(SUPPL. 3):406-413. doi:10.1007/s00586-006-0183-z.

39. Leach MK, Feng Z-Q, Tuck SJ, Corey JM. Electrospinning fundamentals: optimizing solution and apparatus parameters. *J Vis Exp*. 2011;(47):e2494. doi:10.3791/2494.

40. Chang G, Kim HJ, Kaplan D, Vunjak-Novakovic G, Kandel R a. Porous silk scaffolds can be used for tissue engineering annulus fibrosus. *Eur Spine J*. 2007;16(11):1848-1857. doi:10.1007/s00586-007-0364-4.

41. Mizuno H, Roy AK, Vacanti C a, Kojima K, Ueda M, Bonassar LJ. Tissue-engineered composites of anulus fibrosus and nucleus pulposus for intervertebral disc replacement. *Spine (Phila Pa 1976)*. 2004;29(12):1290-1297; discussion 1297-1298. doi:10.1097/01.BRS.0000128264.46510.27.

42. Helen W, Merry CLR, Blaker JJ, Gough JE. Three-dimensional culture of annulus fibrosus cells within PDLLA/Bioglass composite foam scaffolds: assessment of cell attachment, proliferation and extracellular matrix production. *Biomaterials*. 2007;28(11):2010-2020. doi:10.1016/j.biomaterials.2007.01.011.

43. Wan Y, Feng G, Shen FH, Balian G, Laurencin CT. Novel Biodegradable Poly (1 , 8-octanediol malate) for Annulus Fibrosus Regeneration. 2007:1217-1224. doi:10.1002/mabi.200700053.

44. Shao X, Hunter CJ. Developing an alginate/chitosan hybrid fiber scaffold for annulus fibrosus cells. *J Biomed Mater Res A*. 2007;82(3):701-710. doi:10.1002/jbm.a.31030.

45. Bron JL, Helder MN, Meisel H-J, Van Royen BJ, Smit TH. Repair, regenerative and supportive therapies of the annulus fibrosus: achievements and challenges. *Eur Spine J*. 2009;18(3):301-313. doi:10.1007/s00586-008-0856-x.

46. Tedder ME, Liao J, Weed B, et al. Stabilized collagen scaffolds for heart valve tissue engineering. *Tissue Eng Part A*. 2009;15(6):1257-1268. doi:10.1089/ten.tea.2008.0263.

47. Holzapfel GA, Schulze-Bauer CA, Feigl G, Regitnig P. Single lamellar mechanics of the human lumbar anulus fibrosus. *Biomech Model Mechanobiol*. 2005;3(3):125-140. doi:10.1007/s10237-004-0053-8.

48. O'Connell GD, Sen S, Elliott DM. Human annulus fibrosus material properties from biaxial testing and constitutive modeling are altered with degeneration. *Biomech Model Mechanobiol*. 2012;11(3-4):493-503. doi:10.1007/s10237-011-0328-9.

49. O'Connell GD, Guerin HL, Elliott DM. Theoretical and uniaxial experimental evaluation of human annulus fibrosus degeneration. *J Biomech Eng*. 2009;131(11):111007. doi:10.1115/1.3212104.

50. Fung YC. Biomechanics: Mechanical Properties of Living Tissues.

51. Chen EJ, Novakofski J, Jenkins WK, O'Brien WD. Young's Modulus Measurements of Soft Tissues with Application to Elasticity Imaging. 1996;43(1).

52. TrowBridge EA, Black MM, Daniel CL. The mechanical response of glutaraldehyde-fixed bovine pericardium to uniaxial load. *J Mater Sci*. 1985:114-140. http://download-v2.springer.com.libproxy.clemson.edu/static/pdf/749/art%3A10.1007%2FBF00555905.pdf?token2=exp=1428007893~acl=/static/pdf/749/art%253A10.1007%252FBF00555905.pdf*~hmac=bf9472e0671c45569842cfa8af4a78e9f8a152182514d33db3cfdfe90. Accessed April 2, 2015.

53. Keane TJ, Londono R, Turner NJ, Badylak SF. Consequences of ineffective decellularization of biologic scaffolds on the host response. *Biomaterials*. 2012;33(6):1771-1781. doi:10.1016/j.biomaterials.2011.10.054.

54. Ebara. Tensile Properties of Nondegenerate Human Lumbar Anulus Fibrosus. 1996.

55. Wilke H, Neef P, Caimi M, Hoogland T, Claes LE. New In Vivo Measurements of Pressures in the Intervertebral Disc in Daily Life. *Spine (Phila Pa 1976)*. 1999;24(8):755-762. doi:10.1097/00007632-199904150-00005.

56. Iatridis JC, Nicoll SB, Michalek AJ, Walter B a, Gupta MS. Role of biomechanics in intervertebral disc degeneration and regenerative therapies: what needs repairing

in the disc and what are promising biomaterials for its repair? *Spine J*. 2013;13(3):243-262. doi:10.1016/j.spinee.2012.12.002.

57. Nerurkar NL, Elliott DM, Mauck RL. Mechanics of oriented electrospun nanofibrous scaffolds for annulus fibrosus tissue engineering. *J Orthop Res*. 2007;25(8):1018-1028. doi:10.1002/jor.20384.

58. Urban, Roberts. Arthritis Research Therapies. 2003;5:120-130.

59. Timothy E. Hardingham. Cartilage: Aggrecan-Link Protein-Hyaluronan Aggregates. 1998. http://glycoforum.gr.jp/science/hyaluronan/HA05/HA05E.html#top. Accessed April 2, 2015.

60. The American Center for Spine & Neurosurgery. 2015. http://www.acsneuro.com/patient_resources/anatomy. Accessed February 4, 2015.

61. Spine Universe. http://www.spineuniverse.com/. Accessed February 4, 2015.

62. Englewood Orthopedic Associates - Patient Info. http://www.englewoodortho.com/herniated-disc-englewood-ortho.html. Accessed February 4, 2015.

63. Roggia A. Morphopedics-Degenerative Disc Disease. http://morphopedics.wikidot.com/degenerative-disc-disease. Accessed February 4, 2015.

64. Peak Performance Spine & Sports Medicine - Degenerative Disc Disease. 2011. http://peakperformancespine.com/portfolio/degenerative-disc-disease/. Accessed March 4, 2015.

65. Y. Zhu. Contact Stress. http://www.mae.ncsu.edu/zhu/courses/mae316/lecture/5-Contact_Stress_Shig.pdf. Accessed February 4, 2015.